Transient Simulation of Complex High-Speed Channels via Waveform Relaxation

Transient simulation of complex high-speed channels via Waveform Relaxation

Vittorio Loggia, Stefano Grivet-Talocia, *Senior Member, IEEE*, Haisheng Hu

***Abstract*—This paper presents a class of numerical schemes for fast transient simulation of electrically long and complex linear channels terminated by linear or nonlinear networks. The common denominator of all schemes is Waveform Relaxation. Domain decomposition approaches based on Longitudinal and Transverse Partitioning are pursued, leading to various iterative methods characterized by different properties and numerical efficiency. For each scheme, we present a detailed convergence analysis and a set of numerical results obtained on industrial benchmarks. The main contribution of this work is a novel theoretical framework based on a combination of Longitudinal and Transverse Relaxation, leading to particularly efficient simulations when combined with compact channel representations based on Delay-Rational Macromodels. Our prototypal implementation outperforms SPICE solvers, with speedup of up to two orders of magnitude.**

***Index Terms*—Macromodeling, Rational Approximations, Delay Extraction, Scattering Parameters, Transmission Lines, High-Speed Interconnects, Waveform Relaxation, Transverse Partitioning, Longitudinal Partitioning**

I. Introduction

The electrical verification of chip-to-chip communication links requires extensive transient simulations [1], [2]. This kind of analysis is quite demanding, due to several reasons. First, the electrical length of such structures is usually very large. The impulse responses of the channel exploit long memory effects due to the finite propagation speed along the channel path, associated to spurious signal reflections from various discontinuities and terminations. Second, the number of coupled ports that need to be considered is large as well, since all possible signal degradation effects need to be taken into account. Third, typical drivers and receivers for high-speed signaling are nonlinear and dynamic in nature and almost invariably include sophisticated pre-emphasis and equalization features. Accurate and efficient transient analysis of electrically large multiport channels with nonlinear terminations poses significant challenges, which we want to address in this work.

The native characterization of linear multiport channels is usually available as a table of frequency-domain scattering samples. Thus, some form of frequency- to time-domain conversion is required. Leading approaches perform drastic simplifications by assuming linear models for drivers and receivers. This approach enables a time-domain conversion using standard FFT approaches and enables linear convolution-based simulation [1], [2], [3], [4]. Although global metrics such as eye diagram opening and Bit Error Rate (BER) statistics can be computed very fast, the amount of inaccuracy introduced by the linearity assumption is sometimes difficult to assess, thus possibly compromising the reliability and the representativeness of the results.

We concentrate here on circuit-based solution methods, which natively allow the direct inclusion of nonlinear terminations. Time-domain conversion of the channel scattering samples is here performed using a suitable macromodeling approach. Due to the electrical length, standard rational macromodeling is ruled out for obvious complexity reasons [5]–[12]. Standard macromodels based on the Mutliconductor Transmission Line (MTL) topology [13]–[19] are also not adequate, since chip-to-chip links include several discontinuities (vias, connectors, irregular routing) that do not fit in the MTL structure. Therefore, we will adopt the more general Delayed Rational Macromodel (DRM) form [20]–[25].

The port-to-port transfer functions of the channel are represented in DRM's as linear combinations of rational functions weighted by suitable time-delay operators. The former aim at representing attenuation and dispersion effects, while the latter are responsible for a physics-consistent representation of the finite propagation speed along the path, including the effects of multiple discontinuities causing signal reflections. DRM's can be efficiently identified using black-box fitting algorithms from tabulated frequency samples, and several methods are available for checking and enforcing their passivity [26]–[29].

Extensive application of DRM's for channel qualification has been documented in [30], [31], where the transient simulation was performed using standard solvers of the SPICE class. However, there is still a significant margin for improving numerical efficiency. In fact, it can be observed that direct SPICE realizations of interconnect models do not scale well with the number of coupled ports. This is true for wide MTL structures, as documented in [32], [33], [34], but also for more general multiport channels. They are both characterized by a set of small and weakly coupled subsystems, consisting of single interconnects providing direct electrical connection between few (two) ports. This topology calls for Waveform Relaxation (WR) approaches [1], [17], [32]–[51], which first solve each subsystem independently and then update the solution by iteratively correcting the estimates of the coupling terms.

This work presents several Waveform Relaxation approaches for the transient simulation of high-speed channels characterized as DRM's and terminated by nonlinear circuits.

Manuscript received ; revised.

Vittorio Loggia, Stefano Grivet-Talocia and Haisheng Hu are with the Department of Electronics, Politecnico di Torino, Torino 10129, Italy (e-mail: vittorio.loggia@polito.it, stefano.grivet@polito.it, haisheng.hu@polito.it).

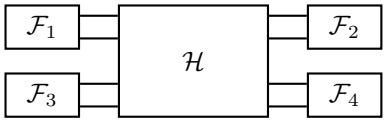

Fig. 1. System topology.

Transverse partitioning [32], [33], [34] is applied to decouple individual channels, and longitudinal partitioning [41], [42] is applied to decouple the individual channels from their terminations. These two approaches have been extensively studied and applied in the context of MTL's. In this work, we propose a combination of the two partitioning schemes into a two-level Waveform Relaxation scheme, which proves particularly efficient when applied to channel models in DRM form. The numerical results show that the proposed schemes outperform SPICE by up to two orders of magnitude in simulation speed. This work provides a complete theoretical framework supporting the preliminary results of [51].

This work is organized as follows. Section II states the main problem, sets the notation, and presents the benchmark structures that will be used for the numerical tests. Section III overviews DRM's in their frequency and time-domain representation and presents the main recursive convolution engine forming the computational core of all schemes. Section IV presents a Waveform Relaxation scheme based on Longitudinal Partitioning (WR-LP), which decouples the channel from its termination networks. Section V introduces another Waveform Relaxation scheme based on Transverse Partitioning (WR-TP), aimed at decoupling individual channels through the introduction of suitable relaxation sources. Section VI combines the WR-LP and WR-TP algorithms into a two-level Waveform Relaxation scheme, which we denote as WR-LPTP. Convergence of all schemes is analyzed, and several transient results demonstrate the accuracy and efficiency of our implementations.

II. Problem statement

This section states the main simulation problem that we address in this work and introduces all the benchmark cases that will be analyzed, highlighting main channel features and termination schemes. The reference structure is a fully-coupled P-port channel terminated by single-ended drivers and receivers. Figure 1 depicts this structure for the case $P = 4$, corresponding to two coupled channels only (all benchmarks that will be analyzed have $P = 18$ ports, see Sec. II-A). We make the assumption that the only coupling between different nets occurs within the channel, with no explicit coupling between individual drivers and receivers. This case is quite common in practical applications. The single terminations can be nonlinear and/or dynamic.

Throughout this work, we will denote with $\boldsymbol{a}(t)$ and $\boldsymbol{b}(t)$ the transient scattering wave vectors that are incident to and reflected by the channel, respectively. We have the following problem formulation

$$\begin{cases} \boldsymbol{b}(t) = \mathbf{h}(t) * \boldsymbol{a}(t) \\ F_q\left(a_q(t); b_q(t); t; \frac{d}{dt}\right) = 0\,, \quad q = 1, \ldots, P \end{cases} \tag{1}$$

where the first row represents the convolution between transient scattering waves entering the channel and the channel impulse response matrix $\mathbf{h}(t)$, and the second row collects all possibly nonlinear and dynamic equations representing drivers and receivers. Both channel and termination equations will be assumed to be explicit in their respective reflected scattering waves. The proposed WR schemes will thus be presented with the more abstract notation

$$\begin{cases} \boldsymbol{b} = \mathcal{H}\,\boldsymbol{a}\,, \\ \boldsymbol{a} = \mathcal{F}\,(\boldsymbol{b})\,, \end{cases} \tag{2}$$

where the linear operator $\mathcal{H}$ represents the channel, and where the termination equations have been written in explicit form through a suitable operator $\mathcal{F}$. The latter is diagonal (it couples only impinging and reflected waves at a single port) but can be nonlinear, dynamic and possibly includes time-varying source terms as in the case of drivers.

Different vector and matrix norms will be used throughout this paper. The notation $\|\ \|$ will stand for the euclidean norm of vectors $\|\boldsymbol{x}\| = (\sum_k |x_k|^2)^{1/2}$ and the corresponding induced (spectral) norm for matrices $\|\mathbf{A}\| = (\lambda_{\max}\{\mathbf{A}^H\mathbf{A}\})^{1/2}$, where $\lambda_{\max}$ is the maximum eigenvalue of its matrix argument. Convergence of WR iterations will be assessed through the norm $\|\boldsymbol{\delta}\|_\infty = \max_{t,k} |\delta_k(t)|$, where k denotes the k-th component and t is the discrete time variable.

A. Benchmark channels

The numerical simulation schemes will be tested and analyzed using a number of industrial benchmark cases (courtesy of IBM). These benchmarks are depicted in Fig. 2. Case I is a simple structure with two coupled lossy transmission line segments with embedded discontinuities due to a via field. The other structures are chip-to-chip links in real products, characterized by various topologies and electrical length. The relevant parameters of the raw specification of each channel (bandwidth, number of ports, and number of available frequency samples for each element of the scattering matrix) are summarized in Table I. A detailed description of the model extraction and characterization for these channels is postponed to Sec. III.

TABLE I
Main parameters of the test cases.

Case	Ports	Samples	Bandwidth
I	18	4096	20 GHz
II	18	1024	20 GHz
III	18	2043	10 GHz
IV	18	1024	20 GHz

B. Termination schemes

We will consider various channel termination schemes, summarized in Table II. Terminations TC-A and TC-C consist of linear Thevenin voltage drivers with a series resistance R_S

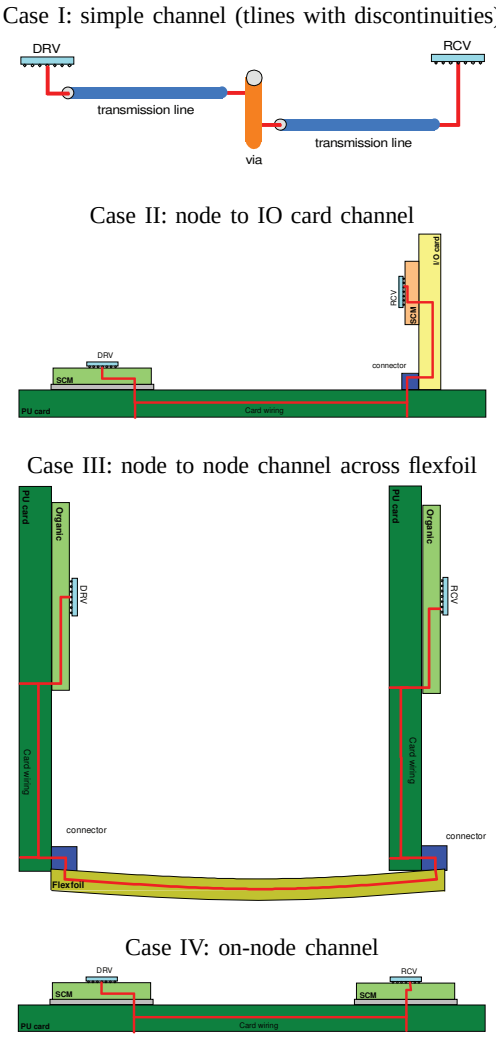

Fig. 2. Graphical illustration of the channel benchmarks.

TABLE II
TERMINATION SCHEMES.

	R_S	C_L	$T_{\mathrm{r,f}}$	T_{bit}	$V_{\max}$
TC-A	40Ω	1pF	66ps	500ps	1.1 V
TC-B	–	1pF	200ps	400ps	1.8 V
TC-C	10Ω	10pF	66ps	500ps	1.1 V

placed at the near-end (odd-numbered) ports, and capacitive receivers C_L at the far-end (even-numbered) ports. Termination TC-B uses for all drivers suitable nonlinear behavioral macromodels of the MπLog class [52]. The driver characteristics can be easily cast in the compact form (1) or (2), second row. A detailed description of these macromodels can be found in [52] and references therein. We remark that this choice for nonlinear terminations is not restrictive, and other behavioral or circuit-based representations can be used.

In all transient simulations, we will excite the victim channel (driver at port 9, receiver at port 10) with a pseudo-random bit sequence (PRBS). Synchronous clock aggressor signals will instead be applied to the near-end (odd-numbered ports except port 9) in order to maximize the induced crosstalk at the victim receiver. Table II lists the main features of the above signals in terms of rise/fall time $T_{\mathrm{r,f}}$, bit time T_{bit}, and voltage swing $V_{\max}$.

III. Delayed Rational Macromodels and Recursive Convolutions

A. Delayed rational macromodels

Each channel structure is known via its sampled scattering matrix $\widehat{\mathbf{H}}_l \in \mathbb{C}^{P\times P}$ at the discrete frequencies ω_l, $l = 1,\ldots,L$. A Delay-Rational Macromodel (DRM) [20]–[25] is given by the closed-form scattering matrix $\mathbf{H}(s)$, with entries

$$H^{i,j}(s) = \sum_{m=0}^{M^{i,j}} Q_m^{i,j}(s) e^{-s\tau_m^{i,j}} + D^{i,j} \tag{3}$$

where s is the Laplace variable, i,j denote output and input port, respectively, corresponding to the selected scattering response, $\tau_m^{i,j}$ are delays corresponding to the various arrival times of the signal reflections induced by an input unit pulse, and

$$Q_m^{i,j}(s) = \sum_{n=1}^{N_m^{i,j}} \frac{R_{mn}^{i,j}}{s - p_{mn}^{i,j}} \tag{4}$$

are rational coefficients representing other effects such as attenuation and dispersion. The case $M^{i,j} = 1$, $\tau_1^{i,j} = 0$ corresponds to a standard (delayless) purely rational macromodel.

The identification of (3) from the samples $\widehat{\mathbf{H}}_l$, i.e., solving

$$\min \left\| \mathbf{H}(j\omega_l) - \widehat{\mathbf{H}}_l \right\|, \tag{5}$$

where the minimum is taken over the unknown delays $\tau_m^{i,j}$ and matrix rational functions $Q_m^{i,j}(s)$ is a very challenging task. However, good solutions via Delayed Vector Fitting (DVF) or Delayed Sanathanan-Koerner (DSK) iterations are available, see [23]. These techniques are based on a two-step algorithm. The first stage consists in the identification of the delays. This task is accomplished by using a time-frequency decomposition of the sampled scattering matrix, which reveals the locations of dominant unknown delays $\tau_m^{i,j}$. Once they are known, a linearized least-squares problem is used for the identification of poles and residues of the rational transfer functions $Q_m^{i,j}(s)$. This second step is a direct generalization of the standard Vector Fitting (VF) algorithm used for lumped models.

Delay-rational curve fitting is not able to preserve the passivity of the raw data per se. This fundamental physical property requires that no energy can be generated by the macromodel under any circumstance. It is well known that non-passive macromodels may lead to unstable results when used in transient simulations, even when their terminations are passive [53], [54]. Therefore, the model must be checked for passivity and, if passivity is violated within some frequency bands, a suitable passivity enforcement process must be applied. In case all poles of all rational coefficients $Q_m^{i,j}(s)$ have a strictly negative real part (this condition is easily enforced by any standard rational identification scheme such as VF, DVF, or DSK), and if $Q_m^{i,j}(s)$ is strictly proper, it can be shown [26] that the model (3) is passive if and only if

$$(\mathbf{I} - \mathbf{H}^H(j\omega)\mathbf{H}(j\omega)) \geqslant 0, \quad \forall\omega \tag{6}$$

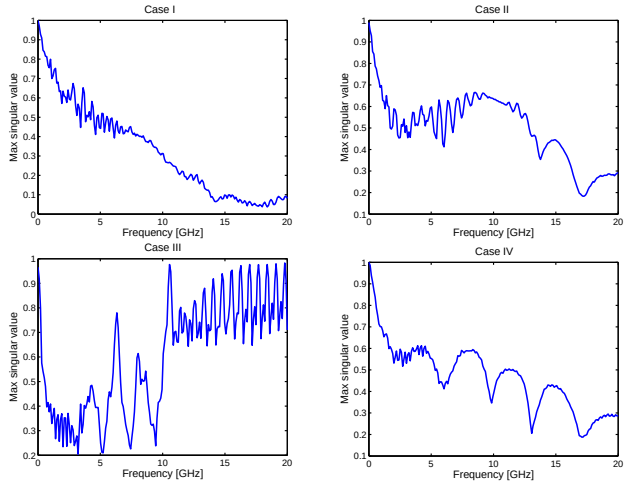

Fig. 3. Maximum singular value plotted versus frequency for all channel models.

or, equivalently, when all the singular values of $\mathbf{S}(j\omega)$ do not exceed one at any frequency. If this condition is violated, passivity enforcement is mandatory. Several approaches are available [26]–[29] for perturbing the model coefficients in order to enforce the condition (6). All DRM's that are used in this work have been checked (see Fig. 3) and are guaranteed passive.

B. Time-domain DRM representation

One of the key ingredients of the proposed WR schemes is the efficient application of the DRM operator (3) to arbitrary time-domain signals. It turns out that this operator has a closed-form representation in time-domain. In general, the application of a DRM operator model to a generic input $\boldsymbol{x}(t)$ leads to a time-domain convolution

$$\boldsymbol{Y}(s) = \mathbf{H}(s) \cdot \boldsymbol{X}(s) \xrightarrow{\mathcal{L}^{-1}} \boldsymbol{y}(t) = \mathbf{h}(t) * \boldsymbol{x}(t)\,, \qquad (7)$$

where $\mathcal{L}^{-1}$ is the inverse Laplace operator. If we consider a single component $y^i(t)$ of the corresponding output, we get the linear superposition

$$y^i(t) = \sum_{j=0}^{P} \int_0^t h^{i,j}(t-\theta) x^j(\theta)\, d\theta \qquad (8)$$

where

$$h^{i,j}(t) = \sum_{m=0}^{M^{i,j}} \sum_{n=1}^{N_m^{i,j}} R_{mn}^{i,j} \mathrm{e}^{p_{mn}^{i,j}\left(t-\tau_m^{i,j}\right)} u(t-\tau_m^{i,j}) + D^{i,j}\delta(t) \qquad (9)$$

is the inverse Laplace transform of (3). Due to the exponential nature of the individual terms in (9), the numerical evaluation of (8) can be formulated as a recursive expression, which can be computed significantly faster than a direct implementation of the integral. As we will show below, this fast evaluation is equivalent to casting (8) as an Infinite Impulse Response (IIR) filter, provided that a uniform sampling of the time axis is performed [55], [56].

C. Recursive convolution

We assume a uniform time discretization step δ, so that all input and output signals are represented and computed over a discrete set of time points $t_k = k\delta$, $k = 0, 1, \ldots$. The inputs $\boldsymbol{x}(t)$ will be represented as piecewise linear signals interpolating their samples $\boldsymbol{x}_k = \boldsymbol{x}(k\delta)$ according to

$$\boldsymbol{x}(t) = \boldsymbol{x}_k \frac{t - t_{k-1}}{\delta} + \boldsymbol{x}_{k-1} \frac{t_k - t}{\delta}\,, \quad \forall t \in [t_{k-1}, t_k]\,, \qquad (10)$$

and similarly for the outputs $\boldsymbol{y}(t)$.

For simplicity, we present the main idea through a scalar impulse response with a single-pole ($\Re\{p\} < 0$) and a single-delay τ

$$h(t) = \mathrm{e}^{p(t-\tau)} u(t-\tau)\,, \qquad (11)$$

and we will drop all superscripts ^{i,j} and subscripts $_{m,n}$. The convolution of this impulse response with an arbitrary input signal $x(t)$, evaluated at $t = t_k$ reads

$$y(t_k) \simeq y_k = u(t_k - \tau) \int_0^{t_k-\tau} \mathrm{e}^{p(t_k-\tau-\theta)} x(\theta)\, d\theta. \qquad (12)$$

Restricting our analysis to the case $t_k \geq \tau$ (if $t_k < \tau$, the corresponding output y_k vanishes), it is straightforward to prove that

$$y_k = \mathrm{e}^{p\delta} y_{k-1} + \int_{t_{k-1}-\tau}^{t_k-\tau} \mathrm{e}^{p(t_k-\tau-\theta)} x(\theta)\, d\theta. \qquad (13)$$

The integral in (13) provides the update to the solution due to the input contribution in the time interval $[t_{k-1} - \tau, t_k - \tau]$. In case the delay τ is an integer multiple of the discretization step δ, the evaluation of (13) is trivial. If instead the delay is arbitrary, special care is needed. To cover both cases, we decompose the delay τ as

$$\tau = \bar{k}\delta + \tau_\epsilon, \quad \text{where} \quad \bar{k} = \left\lfloor \frac{\tau}{\delta} \right\rfloor \qquad (14)$$

denotes the integral part of the delay and where the remainder is such that $\tau_\epsilon < \delta$. Depending on the presence of a remainder $\tau_\epsilon > 0$, the evaluation of (13) may require the values of $x(t)$ also in the interval $[t_{k-\bar{k}-2}, t_{k-\bar{k}-1}]$ in addition to the interval $[t_{k-\bar{k}-1}, t_{k-\bar{k}}]$. Using the linear interpolation scheme in (10), we obtain the following recurrence expression

$$y_k = \alpha_0 y_{k-1} + \beta_0 x(t_{k-\bar{k}}) + \beta_1 x(t_{k-1-\bar{k}}) + \beta_2 x(t_{k-2-\bar{k}})\,, \qquad (15)$$

corresponding to a first-order IIR filter with three input taps and weights

$$\begin{aligned} \alpha_0 &= \mathrm{e}^{w} \\ \beta_0 &= \frac{q - w + \mathrm{e}^{w-q} - 1}{w\,p} \\ \beta_1 &= \frac{-q + w\mathrm{e}^{w} - q\mathrm{e}^{w} + 1 - 2\mathrm{e}^{w-q} + \mathrm{e}^{w}}{w\,p} \\ \beta_2 &= \frac{q\mathrm{e}^{w} + \mathrm{e}^{w-q} - \mathrm{e}^{w}}{w\,p} \end{aligned} \qquad (16)$$

where

$$w = p\,\delta \quad \text{and} \quad q = \tau_\epsilon\, p \qquad (17)$$

If the remainder $\tau_\epsilon = 0$, we have that $q = 0$, $\beta_2 = 0$, and the other coefficients match the results of [9], see also [56]. Thus,

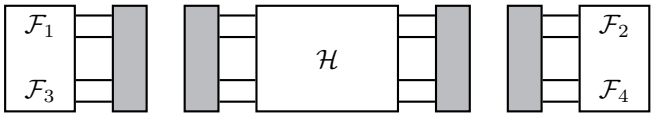

Fig. 4. Graphical illustration of WR-LP partitioning scheme. Gray boxes denote relaxation/decoupling sources.

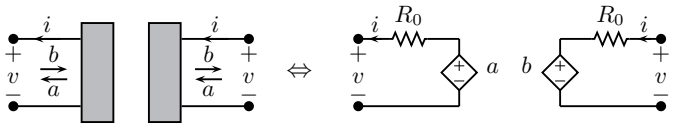

Fig. 5. Definition of the decoupling source for a single interface port.

we see that (16)-(17) generalize standard recurrence relations to the case with delays that are not multiples of the time discretization step.

IV. WR-LP: Waveform Relaxation via Longitudinal Partitioning

In this section, we present a Waveform Relaxation via Longitudinal Partitioning (WR-LP) scheme [41], [42] for the solution of problem (2). A direct solution in time domain would require to solve a fully coupled and possibly non-linear system at any time step for both unknown vectors $\boldsymbol{a}, \boldsymbol{b}$. In order to avoid this operation, we perform a cut at all channel ports in order to separate the channel from its terminations, and we connect to each pair of terminals of both channel and terminations a suitable decoupling source. Figure 4 provides a graphical illustration of the partitioning scheme.

The decoupling sources must be such that the resulting system is fully equivalent to the original one. Considering each port individually, the corresponding decoupling source must "connect" the channel to the corresponding termination circuit by making sure that both incident and reflected scattering waves match at both terminals (Fig. 5, left panel). Using the definition

$$a = v + R_0 i, \qquad b = v - R_0 i \tag{18}$$

of the (voltage) waves a, b in terms of port voltage v and current i and interpreting these as Kirchhoff Voltage Laws, leads to the two circuit branches depicted in the right panel of Fig. 5. If the decoupling resistance R_0 matches the reference port impedance used in the definition of the scattering representation for both channel and terminations, then the solution of all circuit partitions simply requires a forward evaluation of channel and termination operators. Indeed, each port results perfectly matched, implying no reflections from the decoupling networks. We will use this strategy throughout this work.

Waveform Relaxation is now introduced by using the decoupling blocks as relaxation sources. Equivalently, we define an iteration index ν and we relax the instantaneous coupling of the two equations in (2) by delaying one of the terms by one iteration. We obtain the following system, to be solved at any iteration

$$\begin{cases} \boldsymbol{b}_\nu = \mathcal{H}\, \boldsymbol{a}_{\nu-1}\,, \\ \boldsymbol{a}_\nu = \mathcal{F}\,(\boldsymbol{b}_\nu)\,. \end{cases} \tag{19}$$

In this system, the unknowns $\boldsymbol{a}_\nu$ and $\boldsymbol{b}_\nu$ denote the complete time evolution of the incident and reflected waves at iteration ν. Thanks to the decoupling and relaxation process, each equation can be solved independently for the entire time span of the simulation. The iterative process starts with zero initial conditions, $\boldsymbol{a}_0 = \boldsymbol{0}$ and stops when the approximation error estimate

$$\boldsymbol{\delta}_\nu = \boldsymbol{a}_\nu - \boldsymbol{a}_{\nu-1} \tag{20}$$

is below a prescribed threshold.

The scheme is effective when the evaluation of the operators $\mathcal{H}$ and $\mathcal{F}$ is achieved very fast, and when few iterations are required for convergence. This latter issue is addressed in Section IV-A, whereas the efficient application of the operators in time-domain is guaranteed by the derivations in Sec. III, which show that these operators can be cast as recursive convolutions (channel) or recursive and possibly nonlinear filters (terminations). We further remark that the computation of $\boldsymbol{a}_\nu$ using the second row in (19) corresponds to solving each individual termination circuit connected to a linear resistive Thevenin load, as depicted in Fig. 5, with an internal source being known from previous iteration. The pseudocode of the WR-LP scheme is outlined in algorithm 1.

Algorithm 1 Pseudocode of WR-LP algorithm

```
Set initial conditions: a_0 = 0
for ν = 1 to ν_max do
    Apply channel operator: b_ν = H a_{ν-1}
    Solve terminations: a_ν = F(b_ν)
    if ||a_ν − a_{ν-1}||_∞ < ε then
        Break
    end if
end for
```

A. Convergence Analysis

In this section, we analyze the convergence properties of the WR-LP algorithm. The derivations will be performed in the frequency domain under the assumption of linear terminations. We will therefore adopt a different (boldface uppercase) notation, since all matrices and vectors will be assumed to be functions of the Laplace-domain variable s, which will be omitted. The WR-LP system becomes

$$\begin{cases} \boldsymbol{B}_\nu = \mathbf{H}\, \boldsymbol{A}_{\nu-1}\,, \\ \boldsymbol{A}_\nu = \boldsymbol{\Gamma} \boldsymbol{B}_\nu + \boldsymbol{\Upsilon}\,. \end{cases} \tag{21}$$

where $\boldsymbol{A} = \boldsymbol{A}(s)$, $\boldsymbol{B} = \boldsymbol{B}(s)$ are, respectively, incident and reflected scattering waves into the channel, $\mathbf{H} = \mathbf{H}(s)$ is the scattering matrix of the channel, $\boldsymbol{\Gamma} = \boldsymbol{\Gamma}(s)$ is the scattering matrix of the linear terminations, and $\boldsymbol{\Upsilon} = \boldsymbol{\Upsilon}(s)$ denotes the source vector embedded in the terminations.

The exact solution of system (21) can be computed as its fixed point by setting $\nu \to \infty$ and reads

$$\boldsymbol{A}_{\text{exact}} = (\mathbf{I} - \boldsymbol{\Gamma}\mathbf{H})^{-1}\, \boldsymbol{\Upsilon}\,. \tag{22}$$

This solution will be used to verify numerical consistency and convergence of the WR-LP scheme. After $\mathcal{I}$ iterations, we otbain the following solution

$$\boldsymbol{A}_{\mathcal{I}} = \boldsymbol{\Gamma}\mathbf{H}\boldsymbol{A}_{\mathcal{I}-1} + \boldsymbol{\Upsilon} = \sum_{\nu=0}^{\mathcal{I}-1} (\boldsymbol{\Gamma}\mathbf{H})^{\nu} \boldsymbol{\Upsilon} \,. \tag{23}$$

As an error estimate for detecting convergence, we use the difference between two consecutive iterations

$$\begin{aligned} \boldsymbol{\Delta}_{\mathcal{I}} &= \boldsymbol{A}_{\mathcal{I}} - \boldsymbol{A}_{\mathcal{I}-1} \\ &= (\boldsymbol{\Gamma}\mathbf{H})^{\mathcal{I}-1} \boldsymbol{\Upsilon} = (\boldsymbol{\Gamma}\mathbf{H})^{\mathcal{I}-1} (\mathbf{I} - \boldsymbol{\Gamma}\mathbf{H}) \boldsymbol{A}_{\text{exact}} \,. \end{aligned} \tag{24}$$

We can also compute in closed-form the error at the $\mathcal{I}$-th iteration with respect to the exact solution. This error is

$$\boldsymbol{\mathcal{E}}_{\mathcal{I}} = \boldsymbol{A}_{\mathcal{I}} - \boldsymbol{A}_{\text{exact}} = -(\boldsymbol{\Gamma}\mathbf{H})^{\mathcal{I}} \boldsymbol{A}_{\text{exact}} \,. \tag{25}$$

The consistency of the WR-LP algorithm is easily analyzed by taking the limit of the solution for $\mathcal{I} \to \infty$

$$\boldsymbol{A}_{\infty} = \sum_{i=0}^{\infty} (\boldsymbol{\Gamma}\mathbf{H})^{i} \boldsymbol{\Upsilon} \tag{26}$$

which matches (22) when the spectral radius of the iteration operator is less than one at any frequency

$$\rho_{\max}\{\boldsymbol{\Gamma}\mathbf{H}\} = \max_{\omega,i} |\lambda_i\{\boldsymbol{\Gamma}(j\omega)\mathbf{H}(j\omega)\}| < 1 \,, \tag{27}$$

where $\lambda_i\{\cdot\}$ denotes the i-th eigenvalue value of its matrix argument. Condition (27) is easy to check via a suitable sampling process. Since any frequency sampling is not able to check all possible frequencies, a robust implementation should be based on some accuracy-controlled adaptive sampling scheme similar to [57]. The same condition (27) guarantees convergence of the WR-LP scheme, since it implies that both error $\boldsymbol{\mathcal{E}}_{\mathcal{I}}$ and error estimate $\boldsymbol{\Delta}_{\mathcal{I}}$ tend to zero for $\mathcal{I} \to \infty$. Furthermore, the error estimate $\boldsymbol{\Delta}_{\mathcal{I}}$ has the same asymptotic behavior as the exact error $\boldsymbol{\mathcal{E}}_{\mathcal{I}}$ and it is thus proven as a reliable indicator for convergence to be used to stop WR-LP iterations (line 5 in Algorithm 1). Since

$$\rho_{\max}\{\boldsymbol{\Gamma}\mathbf{H}\} \le ||\boldsymbol{\Gamma}\mathbf{H}|| \le ||\boldsymbol{\Gamma}|| \cdot ||\mathbf{H}|| \,, \tag{28}$$

a sufficient condition for convergence of WR-LP is that both channel and terminations are strictly passive, i.e.,

$$||\boldsymbol{\Gamma}|| < 1 \quad \text{and} \quad ||\mathbf{H}|| < 1 \,. \tag{29}$$

These conditions are verified if both channel and terminations are characterized by some amount of dissipativity at any frequency. However, this is not strictly neecessary for WR-LP convergence, since the scheme may converge even if the terminations are not passive, provided that condition (27) holds. More details on convergence of WR-LP schemes as applied to transmission lines can be found in [42].

B. Numerical results

We first investigate the spectral radius of the iteration operators for each channel with different termination schemes, in order to assess the convergence of the WR-LP scheme. Figures 6-7 report the frequency-dependent spectral radius

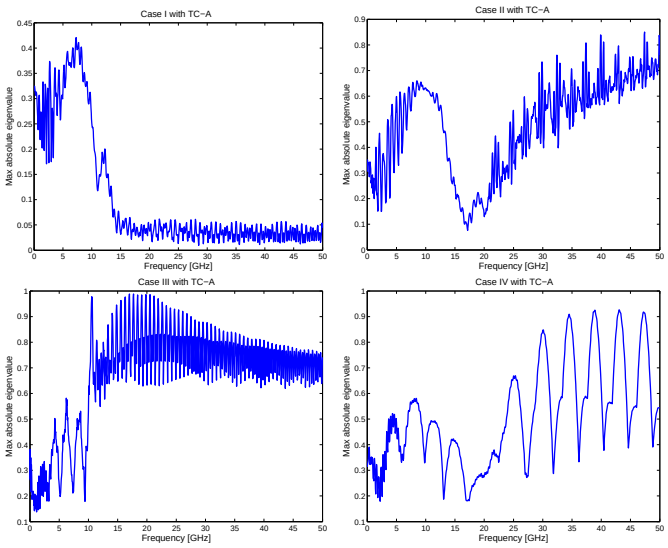

Fig. 6. Spectral radius of operator $\boldsymbol{\Gamma}\mathbf{H}$ plotted versus frequency for all cases with TC-A terminations.

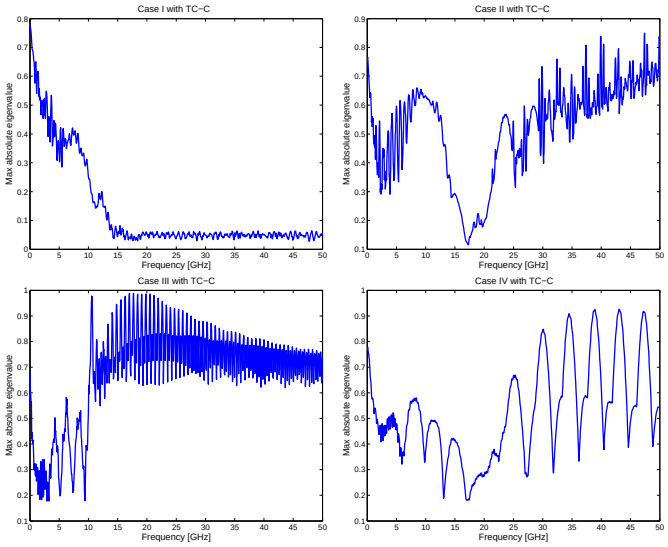

Fig. 7. Spectral radius of operator $\boldsymbol{\Gamma}\mathbf{H}$ plotted versus frequency for all cases with TC-C terminations.

$\rho\{\boldsymbol{\Gamma}\mathbf{H}\}$ for the linear termination cases TC-A and TC-C, respectively. The various panels show that this norm is less than one for all cases, thus implying convergence of WR-LP.

We now illustrate the good convergence properties of the proposed WR-LP scheme. We simulated the Case II channel with terminations TC-A for a 25-bit long excitation. Figure 8 shows the individual waveforms obtained at each WR iteration, so that the fast convergence can be appreciated. Figure 9 reports a validation of this solution with a reference SPICE simulation, no visible difference can be noted.

The same simulation was repeated for all channels, with different linear and nonlinear terminations. The results are summarized in Table III, where simulation times and number of corresponding WR-LP iterations are reported. Analyzing the results, we can see that all cases converge in few iterations to

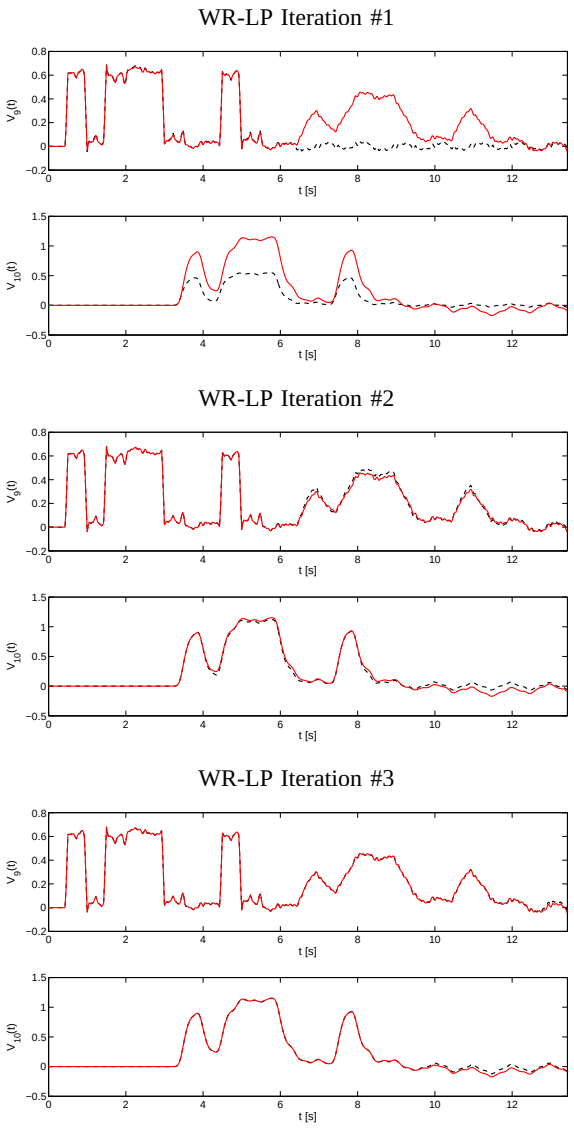

Fig. 8. Case II (TC-A terminations) solution at the first three WR-LP iterations (black dotted line) compared to the exact solution (red line).

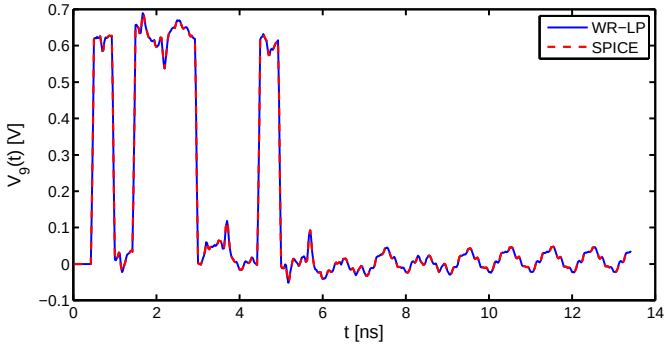

Fig. 9. Case II with TC-A terminations. Comparison between SPICE and WR-LP results for the voltage at the input of victim channel. The maximum deviation among all computed time samples and port voltages is 2.6×10^{-3}.

TABLE III
TIME AND NUMBER ITERATIONS REACHED FOR EACH SIMULATION.

Channel	Terminations	Time, s	Iterations	Error
Case I	TC-A	14.5	7	$< 10^{-6}$
Case II	TC-A	21.4	11	$< 10^{-6}$
Case III	TC-A	7.2	6	$< 10^{-6}$
Case IV	TC-A	13.1	11	$< 10^{-6}$
Case I	TC-B	33.0	8	$< 10^{-6}$
Case II	TC-B	41.1	11	$< 10^{-6}$
Case III	TC-B	23.7	8	$< 10^{-6}$
Case IV	TC-B	27.3	12	$< 10^{-6}$

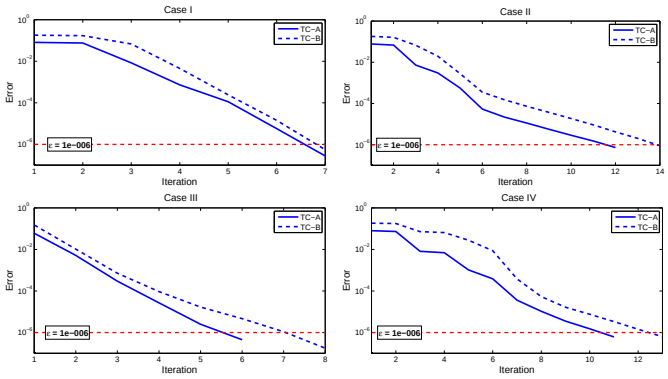

Fig. 10. WR-LP error estimate $\boldsymbol{\delta}_\nu$ plotted vs iteration count for each case and for different termination schemes.

a maximum error less than the prescribed threshold 10^{-6}.

The recursive convolution predicts that the overall simulation time should scale linearly with the number of time steps being computed. In order to validate this conjecture, we performed various simulations of Case II with TC-A terminations using different time step sizes and different numbers of simulated bits. In order to stress the algorithm, the threshold $\epsilon = 10^{-9}$ was used to stop WR-LP iterations. The results, collected in Table IV, confirm this linear dependence.

V. WR-TP: WAVEFORM RELAXATION VIA TRANSVERSE PARTITIONING

In current technologies, high-speed channels for chip-to-chip communication are almost invariably point-to-point connections. A single driver is electrically connected to a single receiver. In case of several interconnects running parallel or in

TABLE IV
SIMULATION TIME AND NUMBER OF WR-LP ITERATIONS REQUIRED FOR DIFFERENT TIME-STEPS AND NUMBER OF SIMULATED BITS.

Bits	δ, ps	Time, s	Iterations
10	25	13.1	10
	12	19.4	12
	6	25.4	12
50	25	66.1	22
	12	116.6	25
	6	218.9	26
100	25	99.7	22
	12	211.7	25
	6	486.9	26

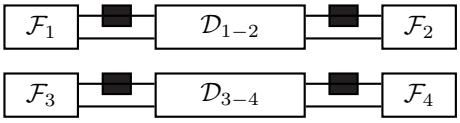

Fig. 11. Graphical illustration of WR-TP partitioning scheme. Black boxes denote relaxation/decoupling sources.

close proximity, there is usually no direct electrical connection between adjacent channels, and inter-channel coupling is only due to near-field electromagnetic interaction. These properties imply a particular block-structure in the scattering matrix of the fully-coupled channel. Direct transmission and reflection coefficients are usually much larger than crosstalk coefficients.

The above considerations lead to the conclusion that the electrical solution of the fully-coupled channel can be interpreted as a perturbation of the solution computed on the set of individual channels with all couplings removed. The amount of perturbation that is required to correct the decoupled solution in order to retrieve the exact solution is expected to be small. These are the main motivations for applying a Transverse Partitioning in the framework of a Waveform Relaxation scheme, which will be denoted as WR-TP.

We proceed as in Sec. IV. We first devise a transverse partitioning scheme [32], [33], [34] in order to transform the original problem as a set of separate subsystems, by recasting the interactions between these subsystems as dedicated coupling sources. Figure 11 provides a graphical illustration of this partitioning. Equivalently, the channel operator $\mathcal{H}$ is decomposed as

$$\mathcal{H} = \mathcal{D} + \mathcal{C} \tag{30}$$

where $\mathcal{D}$ collects all transfer matrix entries representing direct transmission and reflection coefficients, and operator $\mathcal{C}$ collects all crosstalks. Clearly, operator $\mathcal{D}$ is block-diagonal with 2×2 blocks after a suitable permutation depending on the port numbering is applied. Our simulation problem (2) is thus restated as

$$\left\{ \begin{array}{ll} \boldsymbol{\theta} & = \mathcal{C}\, \boldsymbol{a} \\ \boldsymbol{b} & = \mathcal{D}\, \boldsymbol{a} + \boldsymbol{\theta} \\ \boldsymbol{a} & = \mathcal{F}\left(\boldsymbol{b}\right), \end{array} \right. \tag{31}$$

where array $\boldsymbol{\theta}$ collects the crosstalk contributions. If we set $\boldsymbol{\theta} = \mathbf{0}$, all couplings are removed. Note that the termination operator $\mathcal{F}$ in the last row is diagonal.

We are now ready to introduce an iterative scheme based on Waveform Relaxation, using the coupling sources $\boldsymbol{\theta}$ as relaxation terms. Denoting as μ the iteration index, the WR-TP scheme is constructed by delaying the computation of the relaxation sources by one iteration,

$$\left\{ \begin{array}{ll} \boldsymbol{b}_\mu & = \mathcal{D}\, \boldsymbol{a}_\mu + \boldsymbol{\theta}_{\mu-1} \\ \boldsymbol{a}_\mu & = \mathcal{F}\left(\boldsymbol{b}_\mu\right) \\ \boldsymbol{\theta}_\mu & = \mathcal{C}\, \boldsymbol{a}_\mu . \end{array} \right. \tag{32}$$

The system is solved with a suitable initial condition, e.g., $\boldsymbol{\theta}_0 = \mathbf{0}$. The evaluation of both decoupled channel operator $\mathcal{D}$ and relaxation sources $\boldsymbol{\theta}$ is performed via fast recursive convolutions.

System (32) can be formally expressed at the μ-th iteration as

$$\boldsymbol{b}_\mu^q - \mathcal{D}_q \mathcal{F}_q \left(\boldsymbol{b}_\mu^q\right) = \boldsymbol{\theta}_{\mu-1}^q , \qquad q = 1, \ldots, P/2 \tag{33}$$

where q denotes each pair of ports corresponding to the interface of each decoupled channel with its terminations, and where the relaxation source $\boldsymbol{\theta}_{\mu-1}^q$ is known from previous iteration. The inversion of this operator may be difficult in case of nonlinear terminations. However, we will assume throughout this chapter that this inversion, which corresponds to the solution of terminated decoupled channels, can be performed exactly, in order to assess the convergence properties of WR-TP. Section VI will describe our proposed strategy for the numerical computation of this solution. Algorithm 2 highlights the main steps of the WR-TP scheme.

Algorithm 2 Pseudocode of WR-TP algorithm

```
Set initial conditions θ_0 = 0
for μ = 1 to μ_max do
    for q = 1, ..., P/2 do
        Solve q-th channel: b_μ^q − D_q F_q(b_μ^q) = θ_{μ−1}^q
    end for
    Update relaxation sources: θ_μ = C a_μ
    if ||a_μ − a_{μ−1}||_∞ < ε then
        Break
    end if
end for
```

A. Convergence Analysis

In this section, we analyze the convergence properties of the WR-TP scheme. As in Section IV-A, we will assume linear terminations in order to perform this analysis in frequency domain. Therefore, we will denote all unknowns and operators through their frequency-domain representation using uppercase and boldface fonts. The WR-TP system (32) becomes

$$\left\{ \begin{array}{ll} \boldsymbol{B}_\mu & = \mathbf{D}\, \boldsymbol{A}_\mu + \boldsymbol{\Theta}_{\mu-1} \\ \boldsymbol{A}_\mu & = \boldsymbol{\Gamma} \boldsymbol{B}_\mu + \boldsymbol{\Upsilon} \\ \boldsymbol{\Theta}_\mu & = \mathbf{C} \boldsymbol{A}_\mu \end{array} \right. \tag{34}$$

The exact solution of system (34) can be computed as its fixed point by setting $\mu \to \infty$ and reads

$$\boldsymbol{A}_{\text{exact}} = \left(\mathbf{I} - \boldsymbol{\Gamma}(\mathbf{D} + \mathbf{C})\right)^{-1} \boldsymbol{\Upsilon} = \left(\mathbf{I} - \boldsymbol{\Gamma}\mathbf{H}\right)^{-1} \boldsymbol{\Upsilon} , \tag{35}$$

which of course matches (22). After $\mathcal{K}$ iterations, the solution reads

$$\begin{aligned} \boldsymbol{A}_{\mathcal{K}} &= \left(\mathbf{I} - \boldsymbol{\Gamma}\mathbf{D}\right)^{-1} \left(\boldsymbol{\Gamma}\mathbf{C}\boldsymbol{A}_{\mathcal{K}-1} + \boldsymbol{\Upsilon}\right) \\ &= \sum_{\mu=0}^{\mathcal{K}-1} \mathbf{P}^\mu \left(\mathbf{I} - \boldsymbol{\Gamma}\mathbf{D}\right)^{-1} \boldsymbol{\Upsilon} \end{aligned} \tag{36}$$

where operator $\mathbf{P}$ is defined as

$$\mathbf{P} = \left(\mathbf{I} - \boldsymbol{\Gamma}\mathbf{D}\right)^{-1} \boldsymbol{\Gamma}\mathbf{C} . \tag{37}$$

We can compute an estimate of the approximation error by taking the difference of the solution at two consecutive

iterations

$$\begin{aligned} \boldsymbol{\Delta}_{\mathcal{K}} &= \boldsymbol{A}_{\mathcal{K}} - \boldsymbol{A}_{\mathcal{K}-1} \\ &= \mathbf{P}^{\mathcal{K}-1} \left(\mathbf{I} - \boldsymbol{\Gamma}\mathbf{D}\right)^{-1} \boldsymbol{\Upsilon} \\ &= \mathbf{P}^{\mathcal{K}-1} \left(\mathbf{I} - \mathbf{P}\right) \boldsymbol{A}_{\text{exact}} \end{aligned} \tag{38}$$

where (35) has been used. The error between the iterative solution and the exact solution can also be computed and results

$$\boldsymbol{\mathcal{E}}_{\mathcal{K}} = \boldsymbol{A}_{\mathcal{K}} - \boldsymbol{A}_{\text{exact}} = -\mathbf{P}^{\mathcal{K}} \boldsymbol{A}_{\text{exact}} \,. \tag{39}$$

As for the WR-LP scheme of Chapter IV, both error and error estimate have the same asymptotic behavior as a function of the iteration count $\mathcal{K}$, so that the error estimate $\boldsymbol{\Delta}_{\mathcal{K}}$ is a good indicator of convergence. The above derivations show that both consistency and convergence of WR-TP are guaranteed if the spectral radius of the iteration operator is less than one,

$$\rho_{\max}\{\mathbf{P}\} = \max_{\omega,i} \lambda_i\{\mathbf{P}(j\omega)\} < 1 \,. \tag{40}$$

This condition is easily checked by a suitable frequency sampling process. It should be noted that the passivity of both channel and terminations are necessary but not sufficient conditions for convergence, since condition (40) is more restrictive.

Figures 12-13 depicts the spectral radius of the iteration operator versus frequency for all cases and for two different termination schemes. These results show that convergence is expected for both termination schemes on all cases. Although (40) does not necessarily hold in general, this condition was verified on all our benchmarks. These good convergence properties are due to the fact that the cumulative coupling of electromagnetic energy between adjacent channels remains weak when compared to the energy that is traveling on each channel, so that the coupling operator $\mathbf{C}$ is much smaller than the diagonal operator $\mathbf{D}$.

No numerical results are presented in this section, since the WR-TP scheme assumes that the exact solution of (33) is available. The WR-TP scheme is only instrumental for the derivation of the two-level WR-LPTP algorithm, to be presented next.

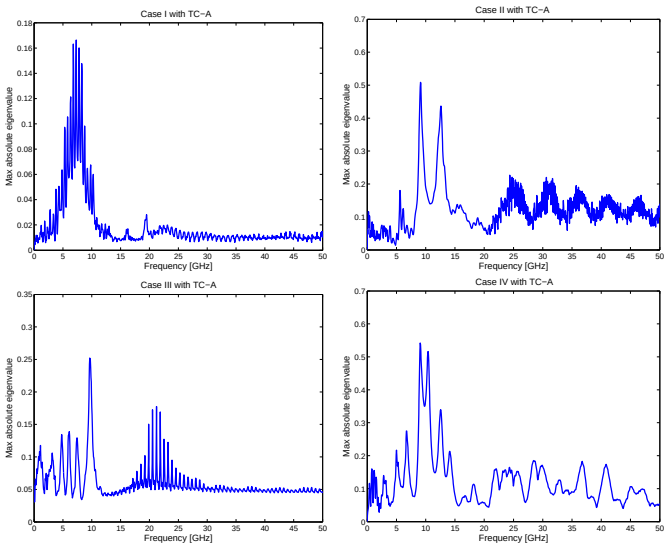

Fig. 12. Spectral radius of WR-TP iteration operator $\mathbf{P}$ plotted versus frequency for all cases with TC-A terminations.

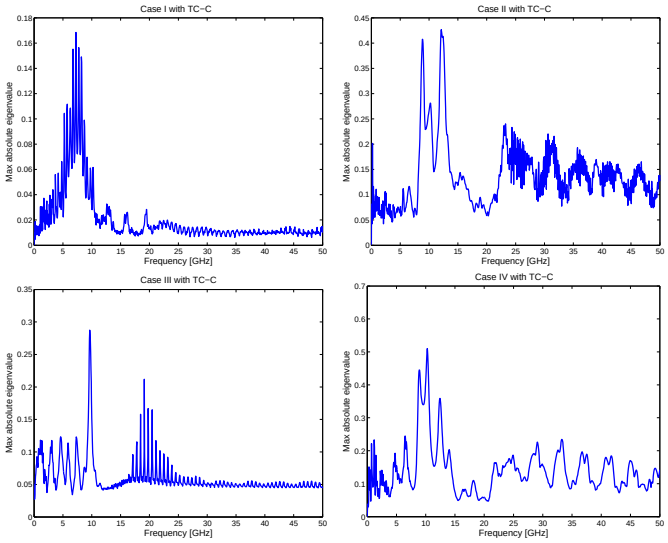

Fig. 13. Spectral radius of WR-TP iteration operator $\mathbf{P}$ plotted versus frequency for all cases with TC-C terminations.

VI. WR-LPTP: Two-level Waveform Relaxation

The WR-LP and WR-TP algorithms presented in Sec. IV and V present both advantages and disadvantages. The WR-LP scheme decouples the channel from its terminations, thus avoiding the requirement of a simultaneous solution of the linear interconnect with its possibly nonlinear loads. However, this scheme does not exploit the particular structure of the channel and is not aware of the presence of small couplings. Therefore, the WR-LP is not expected to scale favorably when increasing the number of coupled channels. The WR-TP scheme is instead well-suited for the analysis of many coupled channels, since the transverse partitioning effectively separates the dominant responses from the small couplings. Thus, this scheme has the potential for very good scalability. Furthermore, its basic steps are independent one of each other, showing good promise for parallelization on a suitable multi-core hardware. Unfortunately, the WR-TP as presented in Section V requires the exact solution of individual channels, which is obviously impossible in general.

In order to combine the advantages of both WR-LP and WR-TP schemes, we propose in this section a two-level Waveform Relaxation algorithm, denoted as WR-LPTP. The starting point is the WR-TP scheme arising from a transverse partitioning. This scheme will form an outer relaxation loop, which is basically identical to (32). A further longitudinal relaxation loop is introduced, according to the WR-LP scheme, in order to solve individual (decoupled) channels. This relaxation will be denoted as inner loop, since it will be performed at each step of the transverse relaxation (outer) loop. A graphical interpretation of the proposed decoupling and relaxation process is provided by Fig. 14, where both inner and outer relaxation sources are highlighted in different

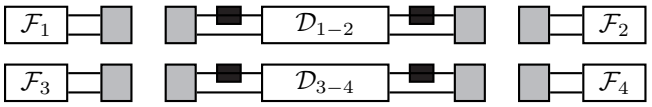

Fig. 14. Graphical illustration of WR-LPTP partitioning scheme. Dark (light) gray boxes denote outer (inner) relaxation sources, respectively.

shades of gray.

For consistency, we will use the same notation that was introduced for the WR-LP and WR-TP schemes. In particular, the outer relaxation index will be denoted as μ, whereas the inner relaxation index will be denoted as ν. At any step of the outer loop, i.e., for fixed μ, the inner loop can be formulated as

$$\begin{cases} \boldsymbol{b}_{\mu,\nu} = \mathcal{D}\,\boldsymbol{a}_{\mu,\nu-1} + \boldsymbol{\theta}_{\mu-1}\,, \\ \boldsymbol{a}_{\mu,\nu} = \mathcal{F}\left(\boldsymbol{b}_{\mu,\nu}\right)\,, \end{cases} \tag{41}$$

where the outer relaxation sources $\boldsymbol{\theta}_{\mu-1}$ are known from previous outer iteration and are set to $\boldsymbol{\theta}_0 = \mathbf{0}$ at the initialization stage $\mu = 0$. Since operator $\mathcal{D}$ is 2×2 block-diagonal and operator $\mathcal{F}$ is diagonal, system (41) can be further split into individual channel contributions as

$$\begin{cases} \boldsymbol{b}^q_{\mu,\nu} = \mathcal{D}_q\,\boldsymbol{a}^q_{\mu,\nu-1} + \boldsymbol{\theta}^q_{\mu-1}\,, \\ \boldsymbol{a}^q_{\mu,\nu} = \mathcal{F}_q\left(\boldsymbol{b}^q_{\mu,\nu}\right)\,, \end{cases} \tag{42}$$

for $q = 1, \ldots, P/2$, where q denotes the port pair pertaining to the q-th channel, as in Section V. System (42) is solved $\forall q$ and for $\nu = 1, \ldots, \mathcal{I}_\mu$ with a suitable initial condition. A good choice for this initial condition is the estimate of the solution that is available at the end of previous outer iteration

$$\boldsymbol{a}_{\mu,0} = \boldsymbol{a}_{\mu-1,\mathcal{I}_{\mu-1}} \tag{43}$$

Once the inner loop has terminated, the outer relaxation sources are updated according to

$$\boldsymbol{\theta}_\mu = \mathcal{C}\,\boldsymbol{a}_{\mu,\mathcal{I}_\mu} \tag{44}$$

and the process is repeated until convergence is achieved. Some considerations on how to choose the appropriate number of inner iterations $\mathcal{I}_\mu$ are postponed to Section VI-A.

Convergence of inner and outer loops is detected by monitoring the respective residual norms with respect to a prescribed threshold ϵ

$$\xi_{\mu,\nu} = ||\boldsymbol{a}_{\mu,\nu} - \boldsymbol{a}_{\mu,\nu-1}||_\infty \tag{45}$$

$$\delta_\mu = ||\boldsymbol{a}_{\mu,\mathcal{I}_\mu} - \boldsymbol{a}_{\mu-1,\mathcal{I}_{\mu-1}}||_\infty\,. \tag{46}$$

The norm $\xi_{\mu,\nu}$ measures the amount of correction that is applied to the solution by the ν-th inner iteration, whereas the norm δ_μ measures the difference between two outer iterations, computed at the end of the inner loop. The actual value of ϵ for the outer iterations should be chosen according to the level of accuracy that is required for the specific application. Different strategies for stopping the inner iterations are presented in Section VI-A. A pseudocode of the proposed scheme is detailed in Algorithm 3.

Algorithm 3 Pseudocode of WR-LPTP algorithm.

```
Set initial conditions θ_0 = a_{1,0} = 0
for μ = 1 to μ_max do
    for ν = 1 to ν_max do
        for q = 1, ..., P/2 do
            Apply channel operator: b^q_{μ,ν} = D_q a^q_{μ,ν-1} + θ^q_{μ-1}
            Solve terminations: a^q_{μ,ν} = F_q (b^q_{μ,ν})
        end for
        if ||a_{μ,ν} − a_{μ,ν-1}||_∞ < ε then
            I_μ = ν, Break
        end if
    end for
    Update outer relaxation sources: θ_μ = C a_μ
    if ||a_{μ,I_μ} − a_{μ-1,I_{μ-1}}||_∞ < ε then
        Break
    end if
    Update initial conditions: a_{μ+1,0} = a_{μ,I_μ}
end for
```

A. Convergence Analysis

We now address the convergence of the WR-LPTP scheme. As for WR-LP and WR-TP, we will work in the frequency domain by assuming linear terminations. The frequency-domain formulation of the main WR-LPTP system (41) reads

$$\begin{cases} \boldsymbol{B}_{\mu,\nu} = \mathbf{D}\,\boldsymbol{A}_{\mu,\nu-1} + \boldsymbol{\Theta}_{\mu-1}\,, \\ \boldsymbol{A}_{\mu,\nu} = \boldsymbol{\Gamma}\boldsymbol{B}_{\mu,\nu} + \boldsymbol{\Upsilon}\,. \end{cases} \tag{47}$$

Let us consider the $\mathcal{K}$-th iteration of the outer loop, and let us assume that we perform a total of $\mathcal{I}_\mathcal{K}$ iterations in the inner loop. We have

$$\boldsymbol{A}_{\mathcal{K},\mathcal{I}_\mathcal{K}} = \boldsymbol{\Gamma}\mathbf{D}\boldsymbol{A}_{\mathcal{K},\mathcal{I}_\mathcal{K}-1} + (\boldsymbol{\Gamma}\boldsymbol{\Theta}_{\mathcal{K}-1} + \boldsymbol{\Upsilon})\,. \tag{48}$$

Following the same derivation that led to (23), we obtain

$$\boldsymbol{A}_{\mathcal{K},\mathcal{I}_\mathcal{K}} = (\boldsymbol{\Gamma}\mathbf{D})^{\mathcal{I}_\mathcal{K}}\,\boldsymbol{A}_{\mathcal{K},0} + \sum_{\nu=0}^{\mathcal{I}_\mathcal{K}-1} (\boldsymbol{\Gamma}\mathbf{D})^\nu\,(\boldsymbol{\Gamma}\boldsymbol{\Theta}_{\mathcal{K}-1} + \boldsymbol{\Upsilon})\,. \tag{49}$$

Using now the initial conditions (43) and the definition of the outer relaxation sources (44), we obtain the expression

$$\boldsymbol{A}_{\mathcal{K},\mathcal{I}_\mathcal{K}} = \mathbf{P}_{\mathcal{I}_\mathcal{K}}\boldsymbol{A}_{\mathcal{K}-1,\mathcal{I}_{\mathcal{K}-1}} + \mathbf{E}_{\mathcal{I}_\mathcal{K}}\,, \tag{50}$$

where

$$\mathbf{P}_{\mathcal{I}_\mathcal{K}} = (\boldsymbol{\Gamma}\mathbf{D})^{\mathcal{I}_\mathcal{K}} + \sum_{\nu=0}^{\mathcal{I}_\mathcal{K}-1} (\boldsymbol{\Gamma}\mathbf{D})^\nu\,\boldsymbol{\Gamma}\mathbf{C} \tag{51}$$

$$\mathbf{E}_{\mathcal{I}_\mathcal{K}} = \sum_{\nu=0}^{\mathcal{I}_\mathcal{K}-1} (\boldsymbol{\Gamma}\mathbf{D})^\nu\,\boldsymbol{\Upsilon}\,. \tag{52}$$

This expression provides an explicit update of the solution between two consecutive outer iterations, taking into account that a finite (and varying) number of inner iterations are performed. Applying recursively this expression until we reach the first outer iteration, for which we have

$$\boldsymbol{A}_{1,\mathcal{I}_1} = \sum_{\nu=0}^{\mathcal{I}_1-1} (\boldsymbol{\Gamma}\mathbf{D})^\nu\,\boldsymbol{\Upsilon} = \mathbf{E}_{\mathcal{I}_1}\,, \tag{53}$$

we obtain

$$\boldsymbol{A}_{\mathcal{K},\mathcal{I}_\mathcal{K}} = \sum_{\mu=0}^{\mathcal{K}-1} \left(\prod_{\alpha=0}^{\mu-1} \mathbf{P}_{\mathcal{I}_{\mathcal{K}-\alpha}} \right) \mathbf{E}_{\mathcal{I}_{\mathcal{K}-\mu}} , \tag{54}$$

where we define the product as 1 if the upper limit is less than the lower limit. This expression is awkward and difficult to interpret, mainly due to the variable number of inner iterations, which makes the operator $\mathbf{P}_{\mathcal{I}_\mathcal{K}}$ iteration-dependent. In order to simplify the discussion, we carry out the convergence analysis for the two modes in which the WR-LPTP scheme will be implemented and tested. These two modes are described and discussed in the following subsections.

1) WR-LPTP–mode 1: First operation mode of WR-LPTP scheme runs the inner iterations until the inner error estimate reaches the convergence threshold, as described in Algorithm 3, line 8. Let us consider the inner error estimate at iteration $\nu = \mathcal{I}_\mu$

$$\begin{aligned} \boldsymbol{\Xi}_\mu &= \boldsymbol{A}_{\mu,\mathcal{I}_\mu} - \boldsymbol{A}_{\mu,\mathcal{I}_\mu-1} \\ &= (\boldsymbol{\Gamma}\mathbf{D} - \mathbf{I})\, \boldsymbol{A}_{\mu,\mathcal{I}_\mu-1} + \boldsymbol{\Gamma}\boldsymbol{\Theta}_{\mu-1} + \boldsymbol{\Upsilon} . \end{aligned} \tag{55}$$

Iteration $\mathcal{I}_\mu$ will break the inner loop if this estimate is sufficiently small

$$||\boldsymbol{\Xi}_\mu|| < \epsilon . \tag{56}$$

If we explicit $\boldsymbol{A}_{\mu,\mathcal{I}_\mu-1}$ from (55) and we apply the inner iteration once more, we obtain the solution estimate that is available when the inner loop stops

$$\boldsymbol{A}_{\mu,\mathcal{I}_\mu} = \mathbf{P}\boldsymbol{A}_{\mu-1,\mathcal{I}_{\mu-1}} + (\mathbf{I} - \boldsymbol{\Gamma}\mathbf{D})^{-1} (\boldsymbol{\Upsilon} - \boldsymbol{\Gamma}\mathbf{D}\, \boldsymbol{\Xi}_\mu) . \tag{57}$$

Setting now $\mu = \mathcal{K}$ and subtracting the exact solution $\boldsymbol{A}_{\text{exact}}$, we obtain the expression of the corresponding approximation error, which after some straightforward algebraic manipulation reads

$$\begin{aligned} \boldsymbol{\mathcal{E}}_\mathcal{K} &= \boldsymbol{A}_{\mathcal{K},\mathcal{I}_\mathcal{K}} - \boldsymbol{A}_{\text{exact}} \\ &= -\sum_{\mu=\mathcal{K}}^{\infty} \mathbf{P}^\mu (\mathbf{I} - \boldsymbol{\Gamma}\mathbf{D})^{-1} \boldsymbol{\Upsilon} \\ &\quad - \sum_{\mu=0}^{\mathcal{K}-1} \mathbf{P}^\mu (\mathbf{I} - \boldsymbol{\Gamma}\mathbf{D})^{-1} \boldsymbol{\Gamma}\mathbf{D}\, \boldsymbol{\Xi}_{\mathcal{K}-\mu} . \end{aligned} \tag{58}$$

This error has two contributions, one deterministic, proportional to the forcing term $\boldsymbol{\Upsilon}$, and one stochastic, which involves all inner iteration residuals $\boldsymbol{\Xi}_\mu$. If the following conditions hold,

$$\rho_{\max}\{\boldsymbol{\Gamma}\mathbf{D}\} < 1 \quad \text{and} \quad \rho_{\max}\{\mathbf{P}\} < 1 , \tag{59}$$

the deterministic part can be made arbitrarily small, and there exists some $\mathcal{K}^*$ such that for $\mathcal{K} \geq \mathcal{K}^*$ we have

$$\boldsymbol{\mathcal{E}}_\mathcal{K} \simeq \sum_{\mu=0}^{\mathcal{K}-1} \mathbf{P}^\mu (\mathbf{I} - \boldsymbol{\Gamma}\mathbf{D})^{-1} \boldsymbol{\Gamma}\mathbf{D}\, \widehat{\boldsymbol{\Xi}}_\mu , \tag{60}$$

where $\widehat{\boldsymbol{\Xi}}_\mu = -\boldsymbol{\Xi}_{\mathcal{K}-\mu}$. An upper bound for the norm of this error is readily obtained under the slightly more restrictive condition $||\mathbf{P}|| < 1$, as

$$\begin{aligned} ||\boldsymbol{\mathcal{E}}_\mathcal{K}|| \leq ||\boldsymbol{\mathcal{E}}_\infty|| &\leq \sum_{\mu=0}^{\infty} ||\mathbf{P}||^\mu || (\mathbf{I} - \boldsymbol{\Gamma}\mathbf{D})^{-1} \boldsymbol{\Gamma}\mathbf{D}|| \, \epsilon \\ &= \frac{|| (\mathbf{I} - \boldsymbol{\Gamma}\mathbf{D})^{-1} \boldsymbol{\Gamma}\mathbf{D}||}{1 - ||\mathbf{P}||} \, \epsilon . \end{aligned} \tag{61}$$

This expression shows that an arbitrarily small error can be achieved by choosing a suitable inner stopping threshold ϵ.

A similar derivation can be applied to the outer error estimate, obtaining

$$\begin{aligned} \boldsymbol{\Delta}_\mathcal{K} &= \boldsymbol{\mathcal{E}}_\mathcal{K} - \boldsymbol{\mathcal{E}}_{\mathcal{K}-1} \\ &= \mathbf{P}^{\mathcal{K}-1} (\mathbf{I} - \boldsymbol{\Gamma}\mathbf{D})^{-1} \boldsymbol{\Upsilon} \\ &\quad - \sum_{\mu=1}^{\mathcal{K}-1} \mathbf{P}^{\mu-1} (\mathbf{P} - \mathbf{I})\, \boldsymbol{\Xi}_{\mathcal{K}-\mu} + \boldsymbol{\Xi}_\mathcal{K} , \end{aligned} \tag{62}$$

Taking $\mathcal{K} \geq \mathcal{K}^*$ so that the deterministic part can be considered negligible, we obtain the following estimate

$$||\boldsymbol{\Delta}_\mathcal{K}|| \leq \left(1 + \frac{||\mathbf{I} - \mathbf{P}||}{1 - ||\mathbf{P}||} \right) || (\mathbf{I} - \boldsymbol{\Gamma}\mathbf{D})^{-1} \boldsymbol{\Gamma}\mathbf{D}|| \, \epsilon , \tag{63}$$

valid if $||\mathbf{P}|| < 1$. Under this condition, both error $\boldsymbol{\mathcal{E}}_\mathcal{K}$ and error estimate $\boldsymbol{\Delta}_\mathcal{K}$ are at most proportional to ϵ with suitable positive and bounded constants.

2) WR-LPTP–mode 2: Second operation mode of WR-LPTP scheme performs a fixed number $\mathcal{I}$ of inner iterations, regardless of the results of the inner convergence test. This assumption leads to a significant simplification with respect to the general derivation of (54), since

$$\mathcal{I}_\mu = \mathcal{I}, \quad \forall \mu \quad \Rightarrow \quad \mathbf{P}_{\mathcal{I}_\mathcal{K}} = \mathbf{P}_\mathcal{I},\ \mathbf{E}_{\mathcal{I}_\mathcal{K}} = \mathbf{E}_\mathcal{I}, \quad \forall \mathcal{K} \tag{64}$$

Equation (54) thus becomes

$$\boldsymbol{A}_{\mathcal{K},\mathcal{I}} = \sum_{\mu=0}^{\mathcal{K}-1} \mathbf{P}_\mathcal{I}^\mu \, \mathbf{E}_\mathcal{I} . \tag{65}$$

Substituting (64) into (51) we obtain an explicit expression of the iteration operator

$$\begin{aligned} \mathbf{P}_\mathcal{I} &= (\boldsymbol{\Gamma}\mathbf{D})^\mathcal{I} + \sum_{\nu=0}^{\mathcal{I}-1} (\boldsymbol{\Gamma}\mathbf{D})^\mathcal{I}\, \boldsymbol{\Gamma}\mathbf{C} \\ &= \mathbf{P} + (\boldsymbol{\Gamma}\mathbf{D})^\mathcal{I} (\mathbf{I} - \mathbf{P}) \end{aligned} \tag{66}$$

It is interesting to note that taking the limit for $\mathcal{I} \to \infty$ leads to

$$\lim_{\mathcal{I}\to\infty} \mathbf{P}_\mathcal{I} = (\mathbf{I} - \boldsymbol{\Gamma}\mathbf{D})^{-1} (\boldsymbol{\Gamma}\mathbf{C}) = \mathbf{P} , \tag{67}$$

$$\lim_{\mathcal{I}\to\infty} \mathbf{E}_\mathcal{I} = (\mathbf{I} - \boldsymbol{\Gamma}\mathbf{D})^{-1} \boldsymbol{\Upsilon} , \tag{68}$$

which match the iteration operator and the forcing term of the WR-TP scheme, see Section V-A. These results hold when

$$\rho_{\max}\{\boldsymbol{\Gamma}\mathbf{D}\} < 1 \tag{69}$$

and confirm the consistency of the WR-LPTP scheme in case the inner loop runs until convergence to its exact solution.

We can now provide explicit expressions for the error of the iterative solution with respect to the exact solution

$$\boldsymbol{\mathcal{E}}_{\mathcal{K},\mathcal{I}} = \boldsymbol{A}_{\mathcal{K},\mathcal{I}} - \boldsymbol{A}_{\text{exact}} = -\mathbf{P}_\mathcal{I}^\mathcal{K} \boldsymbol{A}_{\text{exact}} \tag{70}$$

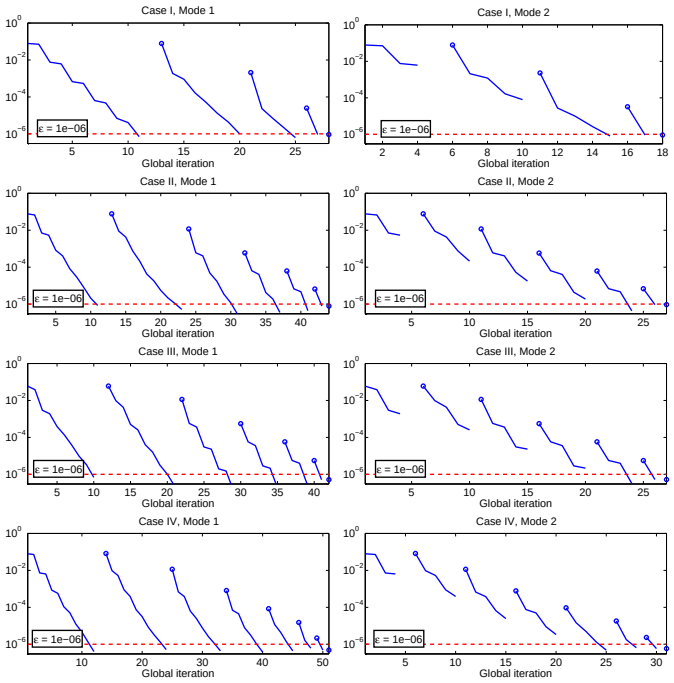

Fig. 15. Evolution of the inner (continuous line) and outer (dots) loop errors through iterations for all cases with TC-A terminations. Left panel refers to WR-LPTP mode 1 (inner loop continues until its convergence). Right panel refers to WR-LPTP mode 2 (inner loops runs for a fixed number $\mathcal{I} = 4$ of iterations).

and for the error estimate at each outer iteration

$$\boldsymbol{\Delta}_{\mathcal{K},\mathcal{I}} = \boldsymbol{A}_{\mathcal{K},\mathcal{I}} - \boldsymbol{A}_{\mathcal{K}-1,\mathcal{I}} = \mathbf{P}_{\mathcal{I}}^{\mathcal{K}-1} \left(\mathbf{I} - \mathbf{P}_{\mathcal{I}}\right) \boldsymbol{A}_{\text{exact}} \,. \quad (71)$$

These expressions show that the condition for convergence of the WR-LPTP–mode 2 scheme is

$$\rho_{\max}\{\mathbf{P}_{\mathcal{I}}\} < 1 \,, \quad (72)$$

which can be checked with a suitable frequency sampling.

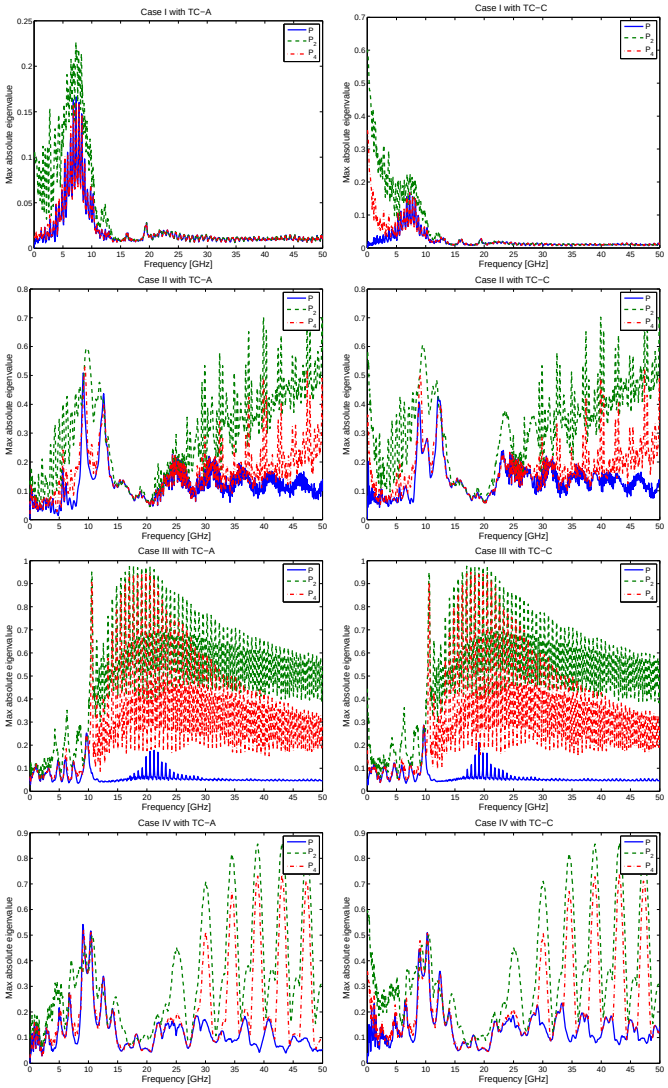

Fig. 16. Spectral radius of operator $\mathbf{P}_{\mathcal{I}}$ for $\mathcal{I} = 2, 4, \infty$ plotted versus frequency for all cases with terminations TC-A (left) and TC-C (right).

B. Numerical results

In this Section, we report some numerical results supporting the hypothesis that the fixed-iteration mode (Mode 2) performs better. An intuitive justification of this conclusion is the following: during outer iterations, the estimates of the inter-channel couplings are affected by some approximation error. Therefore, the exact solution of the inner iteration will not coincide with the exact solution of the original problem, due to the imperfect estimate of these couplings. Therefore, it is not necessary to wait until the inner loop converges to an aggressive threshold, since its target solution is not correct anyway. It is sufficient to perform a few inner iterations so that any correction to the outer relaxation sources performed by previous outer iteration is inherited by the solution of the inner loop. When this condition is fulfilled, it is preferrable to update the outer sources rather than refining an imperfect solution.

A comparison of the two WR-LPTP modes is provided by Fig. 15 for all cases with TC-A terminations (500 bits, time step $\delta = 25$ ps). Each panel reports the evolution of inner loop error estimate (continuous line) and outer loop error estimate (dots). A global iteration count is used in order to simplify visualization and interpretation. In the left panels, the WR-LPTP scheme is run in mode 1, i.e., waiting that the inner loop reaches the convergence threshold before switching to the outer loop. For this analysis, the convergence threshold was set to $\epsilon = 10^{-6}$. In the right panels, the WR-LPTP scheme is run in mode 2 by performing a fixed number of inner iterations, in this case $\mathcal{I} = 4$. It can be seen that for all cases this second mode requires less iterations to reach global convergence. Figure 16 reports the frequency-dependent spectral radius of operator $\mathbf{P}_{\mathcal{I}}$ for all cases and for termination schemes TC-A (left panels) and TC-C (right panels). These figures confirm that all cases are expected to converge.

Table V shows the simulation time and the number of iterations required for each case in the two WR-LPTP modes. This table confirms the better performance of mode 2 with respect to mode 1. A more detailed analysis for Case I is presented in Table VI, where WR-LPTP mode 1 and

TABLE V
SIMULATION TIME AND NUMBER OF GLOBAL ITERATIONS (INNER AND OUTER) REQUIRED BY WR-LPTP MODES 1 AND 2 FOR ALL CASES WITH TC-A TERMINATIONS.

	Mode 1		Mode 2	
	Time, s	Iterations	Time, s	Iterations
Case I	55.8	26	31.4	17
Case II	76.5	40	44.6	26
Case III	55.4	36	34.9	25
Case IV	46.2	45	25.9	29

TABLE VI
CASE I WITH TC-A TERMINATIONS. SIMULATION TIME AND NUMBER OF ITERATIONS REQUIRED FOR DIFFERENT VALUES OF INNER ITERATIONS $\mathcal{I}$ (MODE 2 ONLY) AND STOPPING THRESHOLD ϵ. THE GLOBAL NUMBER OF ITERATIONS IS PROVIDED TOGETHER WITH THE NUMBER OF OUTER ITERATIONS (WITHIN BRACKETS).

ϵ	Mode	$\mathcal{I}$	Time, s	Iterations
10^{-4}	1	–	28.7	14(3)
10^{-4}	2	2	25.2	15(5)
10^{-4}	2	4	20.3	12(3)
10^{-8}	1	–	95.5	45(6)
10^{-8}	2	2	41.4	26(9)
10^{-8}	2	4	48.4	24(6)

mode 2 are compared with different values of the convergence threshold ϵ and number of inner iterations $\mathcal{I}$ (for mode 2 only). The table shows that mode 2 with $\mathcal{I} = 4$ iterations provides the best results. Using less inner iterations in mode 2 is not effective and leads to a larger number of global iterations. Figure 17 reports for all cases the dependence of total runtime on the number of inner iterations $\mathcal{I}$ in the WR-LPTP mode 2 scheme. The minimum runtime is achieved in all cases for $\mathcal{I} = 4$, which can thus be considered as optimal.

The detailed behavior of the solution at different inner/outer iterations is depicted in Figure 18 for Case II with terminations TC-B, i.e. with nonlinear driver models. These plots demonstrate that the final solution is indeed achieved by applying small iterative perturbations. This provides a posteriori justification for the Waveform Relaxation approach that we pursue in this work.

We conclude with a SPICE validation. Figure 19 compares

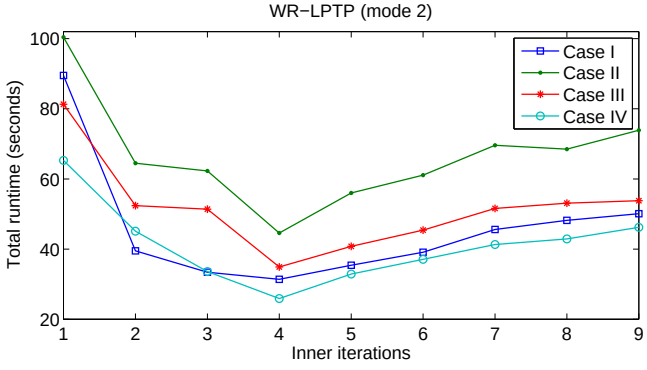

Fig. 17. Total runtime (seconds) required by WR-LPTP (mode 2) scheme to simulate a 500-bit sequence, using different values of inner iterations $\mathcal{I}$.

TABLE VII
COMPARISON OF SIMULATION TIMES (IN SECONDS) REQUIRED BY SPICE, WR-LP, AND WR-LPTP (MODE 1) WITH $\epsilon = 10^{-4}$.

Case	SPICE	WR-LP	WR-LPTP
Case I	807	162.9	28.7
Case II	743	142.1	38.0
Case III	822	116.8	25.4
Case IV	456	96.7	19.6

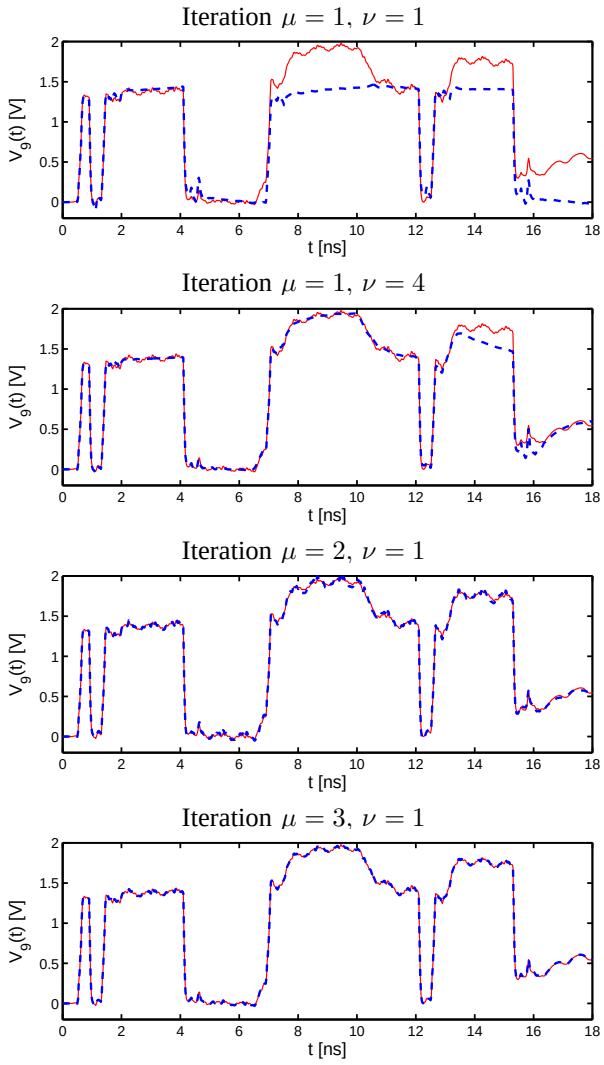

Fig. 18. Case II with TC-B terminations. Solution at various WR-TPLP iterations (blue dashed line) compared to the exact solution (red line).

the transient voltage at the victim channel terminations (Case II with TC-A terminations) computed by SPICE and by our WR-LPTP scheme. The waveforms are not distinguishable on this scale. Table VII reports a comparison of the simulation times reqired by SPICE and by WR-LPTP scheme for all cases. A major speedup is observed, although a prototypal implementation of WR-LPTP in Matlab has been used. This speedup is justified by the special treatment of the weak inter-channel couplings by WR-LPTP, while SPICE does not exploit the particular structure of the channel model in its global MNA formulation. Table VII also reports the runtime for the WR-

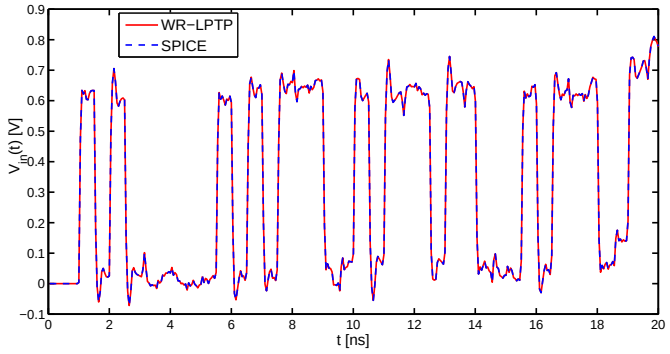

Fig. 19. Case II with TC-A terminations. Comparison between SPICE and WR-LPTP results for input port of victim channel. The maximum error among all computed time samples and all responses is 2.11×10^{-3}.

LP scheme, which results competitive with respect to SPICE but much less efficient than the proposed WR-LPTP two-level relaxation.

VII. Conclusions

This paper introduced three Waveform Relaxation (WR) schemes for transient simulation of complex multiport channels with possibly nonlinear terminations. These schemes are based on a longitudinal and/or transverse partitioning of the structure through suitable decoupling sources, which are relaxed through an iterative process. All schemes are consistent. A detailed linear convergence analysis has been performed, showing that the necessary and sufficient condition for convergence is the strict unitary boundedness of the spectral radius of the WR iteration operator.

Convergence is monitored through an error indicator based on a comparison between the solution at two successive WR iterations. We proved that this indicator has the same asymptotic decay rate as the error with respect to the exact solution. This in turns prevents the WR scheme from stopping the iterations as a result of false convergence detection, as for the case of local minima.

The numerical results show that the so-called WR-LPTP scheme, which combines both longitudinal and transverse partitioning in a two-level relaxation loop, is able to compute the transient solution significantly faster than SPICE-based solvers, due to its ability to exploit the particular structure of the channel coupling terms. Thus, there is a very good promise for routine application of the proposed schemes for the electrical verification of channel transmission in present and future industrial design flows. Even if the bandwidth was limited to 20 GHz for most benchmarks that were analyzed in this work, there is no obvious limitation that would prevent application of our proposed schemes with higher-frequency channel models. We also remark that the WR-LPTP scheme can be easily extended to the case of differential or even fully-coupled driver/receiver networks (e.g., through their power delivery networks), known either via circuit-based or behavioral representations. In these cases, the operator $\mathcal{F}$ in (2) would become block-diagonal or even full. However, thanks to the longitudinal partitioning, such terminations would be solved independently from the channel at each WR iteration, thus allowing direct application of transverse channel partitioning and relaxation, and therefore inheriting the main advantages of the proposed two-level scheme.

Applicability of proposed WR schemes is subject to a convergence condition, which is easy to check via frequency sampling. We have verified that this condition is indeed fulfilled for all benchmark cases we considered. This is due to two fundamental facts. First, inter-channel couplings are usually much smaller than direct transmission and reflection coefficients. This leads to practically a diagonal dominance of the channel scattering matrices, which is functional to the condition for convergence. Second, the terminations typically used in high-speed signaling are always matched or nearly matched to the channel, at least on one end of each interconnect. This leads to small signal reflections from the terminations into the channel and contributes positively to the global convergence of the relaxation loops.

Despite the above considerations, it is conceivable that highly reactive ad hoc terminations can be found such that the proposed WR schemes do not converge. These terminations will likely be far from application interest. However, the development of suitable countermeasures for ensuring convergence in the general case, represents an interesting theoretical challenge. In addition, our present convergence analysis is only valid for linear terminations. Extension of these results to the more general nonlinear case is under way. Our future work will then be devoted to broaden the scope and the applicability of the presented WR schemes in the direction pointed by [50], as well as further improving their efficiency through dedicated parallel implementations for multicore hardware.

VIII. Acknowledgement

The Authors are grateful to Dr. Kaller (IBM) for providing the channel characterization used in the paper. This work was supported in part by the Italian Ministry of University (MIUR) under a Program for the Development of Research of National Interest (PRIN grant #2008W5P2K).

References

[1] W. T. Beyene, “Applications of Multilinear and Waveform Relaxation Methods for Efficient Simulation of Interconnect-Dominated Nonlinear Networks,” *Advanced Packaging, IEEE Transactions on*, vol. 31, no. 3, pp. 637–648, Aug. 2008.

[2] W. T. Beyene, C. Madden, Jung-Hoon Chun, Haechang Lee, Y. Frans, B. Leibowitz, Ken Chang, Namhoon Kim, Ting Wu, G. Yip, R. Perego, “Advanced Modeling and Accurate Characterization of a 16 Gb/s Memory Interface,” *Advanced Packaging, IEEE Transactions on*, vol. 32, no. 2, pp. 306–327, May 2009.

[3] G. Balamurugan, B. Casper, J. E. Jaussi, M. Mansuri, F. O’Mahony, J. Kennedy, “Modeling and Analysis of High-Speed I/O Links,” *Advanced Packaging, IEEE Transactions on*, vol. 32, no. 2, pp. 237–247, May 2009.

[4] A. Sanders, “Statistical Simulation of Physical Transmission Media,” *Advanced Packaging, IEEE Transactions on*, vol. 32, no. 2, pp. 260–267, May 2009.

[5] B. Gustavsen, A. Semlyen, “Rational approximation of frequency responses by vector fitting”, *IEEE Trans. Power Delivery*, Vol. 14, N. 3, July 1999, pp. 1052–1061.

[6] B. Gustavsen, A. Semlyen, “A robust approach for system identification in the frequency domain”, *IEEE Trans. Power Delivery*, Vol. 19, N. 3, July 2004, pp. 1167–1173.

[7] D. Deschrijver, B. Haegeman, T. Dhaene, "Orthonormal Vector Fitting: A Robust Macromodeling Tool for Rational Approximation of Frequency Domain Responses", *IEEE Trans. Adv. Packaging*, vol. 30, pp. 216–225, May 2007.

[8] S. Grivet-Talocia, M. Bandinu, "Improving the Convergence of Vector Fitting in Presence of Noise", *IEEE Transactions on Electromagnetic Compatibility*, vol. 48, n. 1, pp. 104-120, February, 2006.

[9] S. Grivet-Talocia, "Package Macromodeling via Time-Domain Vector Fitting", *IEEE Microwave and Wireless Components Letters*, Vol. 13, no. 11, November 2003.

[10] W. Beyene, J. Schutt-Ainé, "Accurate Frequency-Domain Modeling and Efficient Circuit Simulation of High-Speed Packaging Interconnects", *IEEE Trans. Microwave Theory Tech.*, vol. 45, pp. 1941-1947, Oct. 1997

[11] K. L. Choi, M. Swaminathan, "Development of Model Libraries for Embedded Passives Using Network synthesis", *IEEE Trans. Circuits and Systems II*. vol. 47, pp. 249–260, Apr. 2000.

[12] M. Elzinga, K. Virga, J. L. Prince, "Improve Global Rational Approximation Macromodeling Algorithm for Networks Characterized by Frequency-Sampled Data", *IEEE Trans. Microwave Theory Tech.*, vol. 48, pp. 1461–1467, Sept. 2000

[13] C. Paul, *Analysis of Multiconductor Transmission Lines*. John Wiley & Sons, Inc. New York, NY, USA, 1994.

[14] S. Lin and E. S. Kuh, "Transient simulation of lossy interconnects based on the recursive convolution formulation," *IEEE Trans. Circuits Systems I*, vol. 39, pp. 879-892, Nov. 1992.

[15] S. Grivet-Talocia, H. M. Huang, A. E. Ruehli, F. Canavero, I. M. Elfadel, "Transient Analysis of Lossy Transmission Lines: an Effective Approach Based on the Method of Characteristics," *IEEE Trans. Advanced Packaging*, pp. 45–56, vol. 27, n. 1, Feb. 2004.

[16] D. B. Kuznetsov and J. E. Schutt-Ainé, "Optimal transient simulation of transmission lines," *IEEE Trans. Circuits Systems I*, vol. 43, pp. 110-121, Feb. 1996.

[17] F. Y. Chang, "The generalized method of characteristics for waveform relaxation analysis of lossy coupled transmission lines," *IEEE Trans. Microwave Theory Tech.*, vol. 37, pp. 2028-2038, Dec. 1989.

[18] F. C. M. Lau, "Improvements in the Waveform Relaxation Method Applied to Transmission Lines", *IEEE Transactions on Computer-Aided Design of Integrated Circuits and Systems*, Vol.13, No.11, Nov.1994, pp.1409–1412.

[19] N. M. Nakhla, A. Dounavis, R. Achar, M. S. Nakhla, "DEPACT: delay extraction-based passive compact transmission-line macromodeling algorithm," *IEEE Trans. On Advanced Packaging*, vol. 28, pp. 13-23, Feb. 2005.

[20] S. Grivet-Talocia, "Delay-based macromodels for long interconnects via time-frequency decompositions," in *IEEE* 15^{th} *Topical Meeting on Electrical Performance of Electronic Packaging, Scottsdale, Arizona*, pp. 199–202, Oct. 23–25, 2006.

[21] A. Charest, D. Saraswat, M. Nakhla, R. Achar, N. Soveiko, "Compact Macromodeling of High-Speed Circuits via Delayed Rational Functions," *IEEE Microwave and Wireless Components Letters* Vol. 17, No. 12, pp. 828–830, Dec. 2007.

[22] A. Charest, M. Nakhla, R. Achar, "Delay Extracted Stable Rational Approximations for Tabulated Networks With Periodic Reflections," *IEEE Microwave and Wireless Components Letters*, Vol. 19, No. 12, Dec 2009, pp. 768–770.

[23] A. Chinea, P. Triverio, S. Grivet-Talocia, "Delay-Based Macromodeling of Long Interconnects from Frequency-Domain Terminal Responses," *IEEE Transactions on Advanced Packaging*, Vol. 33, No. 1, pp. 246–256, Feb. 2010.

[24] P. Triverio, S. Grivet-Talocia, A. Chinea, "Identification of highly efficient delay-rational macromodels of long interconnects from tabulated frequency data," *IEEE Transactions on Microwave Theory and Techniques*, vol. 58, no. 3, pp. 566–577, 2010.

[25] A. Charest, M. Nakhla, R. Achar, D. Saraswat, N. Soveiko, I. Erdin, "Time Domain Delay Extraction-Based Macromodeling Algorithm for Long-Delay Networks," *IEEE Transactions on Advanced Packaging*, Vol. 33, No. 1, pp. 219–235, Feb. 2010.

[26] A. Charest, M. Nakhla, R. Achar, "Scattering Domain Passivity Verification and Enforcement of Delayed Rational Functions," *IEEE Microwave and Wireless Components Letters*, Vol. 19, No. 10, Oct. 2009, pp. 605–607.

[27] A. Chinea, S. Grivet-Talocia, P. Triverio, "On the performance of weighting schemes for passivity enforcement of delayed rational macromodels of long interconnects," in *IEEE* 18^{th} *Conf. on Electrical Performance of Electronic Packaging and Systems*, Portland (Tigard), Oregon, Oct. 19–21, 2009.

[28] A. Charest, M. Nakhla, R Achar, C. Chen, "Passivity verification and enforcement of delayed rational function macromodels from networks characterized by tabulated data," in *IEEE Workshop on Signal Propagation on Interconnects, 2009. SPI'09*, pp. 1–4, May 12–15, 2009.

[29] A. Chinea, S. Grivet-Talocia, D. Deschrijver, T. Dhaene, L. Knockaert, "On the construction of guaranteed passive macromodels for high-speed channels," *Design, Automation and Test in Europe (DATE 10)*, Dresden (Germany), pp. 1142-1147, March 8-12, 2010.

[30] A. Chinea, P. Triverio, and S. Grivet-Talocia, "Passive delay-based macromodels for signal integrity verification of multi-chip links," in *14th IEEE Workshop on Signal Propagation on Interconnects, Hildesheim, Germany*, May 9–12, 2010.

[31] A. Chinea, S. Grivet-Talocia, H. Hu, P. Triverio, D. Kaller, C. Siviero, M. Kindscher, "Signal Integrity Verification of Multi-Chip Links using Passive Channel Macromodels," *IEEE Transactions on Advanced Packaging*, 2011, to appear.

[32] N. Nakhla, A. Ruehli, M. Nakhla, R. Achar and C. Chen, "Waveform relaxation techniques for simulation of complex interconnects with frequency-dependent parameters", *IEEE 14-th Topical Meeting on Electrical Performance of Electronic Packaging (EPEP)*, Oct. 2005, pp. 47–50.

[33] N. M. Nakhla, A. E. Ruehli, M. S. Nakhla, R. Achar, "Simulation of coupled interconnects using waveform relaxation and transverse partitioning," *IEEE Transactions on Advanced Packaging*, vol. 29, no. 1, pp. 78–87, Feb. 2006

[34] D. Paul, N. M. Nakhla, R. Achar, M. S. Nakhla, "Parallel Simulation of Massively Coupled Interconnect Networks," *IEEE Transactions on Advanced Packaging*, vol. 33, no. 1, pp. 115–127, Feb. 2010.

[35] E. Lelarasmee, "The Waveform Relaxation Method for Time Domain Analysis of Large Scale Integrated Circuits: Theory and Applications", *EECS Department University of California, Berkeley Technical Report No. UCB/ERL M82/40 1982*.

[36] E. Lelarasmee, A. E. Ruehli, A. L. Sangiovanni-Vincentelli, "The Waveform Relaxation Method for Time-Domain Analysis of Large Scale Integrated Circuits", *IEEE Transactions on Computer-Aided Design of Integrated Circuits and Systems*, Vol. 1, N. 3, July 1982, pp. 131–145.

[37] P. Debefve, J. Beetem, W. Donath, H. Y. Hsieh, F. Odeh, A. E. Ruehli, P. Wolff, Sr., and J. White, "A large-scale MOSFET circuit analyzer based on waveform relaxation," *IEEE Int. Conf. Computer Design*, Rye, NY, Oct. 1984.

[38] J. K. White and A. L. Sangiovanni-Vincentelli, *Relaxation Technique for the Simulation of VLSI Circuits*. Norwell, MA: Kluwer Academic, 1987.

[39] A. E. Ruehli, Ed., *Circuit Analysis, Simulation and Design, Part 2*, Elsevier Science, North Holland, 1987.

[40] P. Saviz, O. Wing, "Circuit Simulation by Hierarchical Waveform Relaxation," *IEEE Transactions on Computer-Aided Design of Integrated Circuits and Systems*, Vol. 12, N. 6, June 1993, pp. 845–860.

[41] M. Gander, M. Al-Khaleel, A. E. Ruehli; "Waveform Relaxation Technique for Longitudinal Partitioning of Transmission Lines,"in *IEEE* 15^{th} *Topical Meeting on Electrical Performance of Electronic Packaging, Scottsdale, Arizona*, pp. 207–210, Oct. 23–25, 2006.

[42] M. J. Gander, M. Al-Khaleel, A. E. Ruehli, "Optimized Waveform Relaxation Methods for Longitudinal Partitioning of Transmission Lines," *IEEE Trans. on Circuits and Systems I: Regular Papers*, vol. 56, no. 8, pp. 1732–1743, Aug. 2009.

[43] R. Wang, O. Wing, "Transient Analysis of Dispersive VLSI Interconnects Terminated in Nonlinear Loads", *IEEE Transactions on Computer-Aided Design*, Vol.11, N.10, Oct.1992, pp. 1258–1277.

[44] A. Lumsdaine, M. W. Reichelt, J. M. Squyres, J. K. White, "Accelerated Waveform Methods for Parallel Transient Simulation of Semiconductor Devices", *IEEE Transactions on Computer-Aided Design of Integrated Circuits and Systems*, Vol. 15, N. 7, July 1996, pp. 716–726.

[45] G. D. Gristede, A. E. Ruehli, C. A. Zukowski, "Convergence Properties of Waveform Relaxation Circuit Simulation Methods", *IEEE Transactions on Circuits and Systems-I: Fundamental Theory and Applications*, Vol.45, No.7, July 1998, pp. 726–738.

[46] Yao-Lin Jiang, "A General Approach to Waveform Relaxation Solutions of Nonlinear Differential-Algebraic Equations: The Continuous-Time and Discrete-Time Cases", *IEEE Transactions on Circuits and Systems-I: Regular Papers*, Vol.51, No.9, Sept.2004, pp. 1770–1780.

[47] I. M. Elfadel, "Convergence of Transverse Waveform Relaxation for the Electrical Analysis of Very Wide Transmission Line Buses", *IEEE Transactions on Computer-Aided Design of Integrated Circuits and Systems*, Vol.28, No.8, 2009, pp.1150–1161.

[48] N. Nakhla, A. E. Ruehli, M. S. Nakhla, R. Achar, C. Chen, "Waveform Relaxation Techniques for Simulation of Coupled Interconnects With

Frequency-Dependent Parameters", *IEEE Transactions on Advanced Packaging*, Vol.30, N.2, 2007, pp. 257–269.
[49] M. J. Gander, A. E. Ruehli, "Optimized Waveform Relaxation Methods for RC Type Circuits", *IEEE Transactions on Circuits and Systems I: Regular Papers*, Vol.51, N.4, April 2004, pp. 755–768.
[50] M. J. Gander, A. E. Ruehli, "Optimized waveform relaxation solution of electromagnetic and circuit problems", in *IEEE 19th Conference on Electrical Performance of Electronic Packaging and Systems (EPEPS)*, 25–27 Oct. 2010, Austin, TX, USA, pp. 65–68.
[51] V. Loggia and S. Grivet-Talocia, "A two-level waveform relaxation approach for fast transient simulation of long high-speed interconnects," in *IEEE* 19^{th} *Topical Meeting on Electrical Performance of Electronic Packaging and Systems (EPEPS 2010), Austin, TX*, October 24–27, 2010.
[52] I. S. Stievano, I. A. Maio, F. G. Canavero, "M[pi]log, Macromodeling via Parametric Identification of Logic Gates," *IEEE Transactions on Advanced Packaging*, Vol. 27, No. 1, pp. 15–23, Feb. 2004.
[53] P. Triverio, S. Grivet-Talocia, M. S. Nakhla, F. Canavero, R. Achar, "Stability, Causality, and Passivity in Electrical Interconnect Models," *IEEE Transactions on Advanced Packaging*, Vol. 30, No. 4, pp. 795–808, Nov. 2007.
[54] S. Grivet-Talocia, "On Driving Non-passive Macromodels to Instability," *International Journal of Circuit Theory and Applications*, Vol. 37, No. 8, pp. 863–886, Oct. 2009.
[55] A. V. Oppenheim, R. W. Schafer, *Digital Signal Processing*, Prentice Hall, Upper Saddle River, NJ, 1999
[56] A. Semlyen and A. Dabuleanu, "Fast and accurate switching transient calculations on transmission lines with ground return using recursive convolutions", *IEEE Trans. Power App. Syst.*, vol. PAS-94, no. 2, pt. 1, pp. 561–575, Mar./Apr. 1975.
[57] S. Grivet-Talocia, "An Adaptive Sampling Technique for Passivity Characterization and Enforcement of Large Interconnect Macromodels," *IEEE Transactions on Advanced Packaging*, vol. 30, n. 2, pp. 226-237, May 2007.

PLACE PHOTO HERE

Vittorio Loggia received the B.Sc. and M.Sc. (summa cum laude) degrees in Electronics Engineering from the Politecnico di Torino, Italy, in 2007 and 2009, respectively. He is currently working towards a Ph.D. degree in Electromagnetic Compatibility Group, Politecnico di Torino, Italy. His research interests concern modeling and simulation of high-complexity interconnects, with emphasis on Waveform Relaxation algorithms. He was selected for the IBM EMEA Best Student Recognition Event in 2009.

PLACE PHOTO HERE

Stefano Grivet-Talocia (M'98–SM'07) received the Laurea and the Ph.D. degrees in electronic engineering from Politecnico di Torino, Italy. From 1994 to 1996, he was with the NASA/Goddard Space Flight Center, Greenbelt, MD, USA. Currently, he is an Associate Professor of Circuit Theory with Politecnico di Torino. His research interests are in passive macromodeling of lumped and distributed interconnect structures, modeling and simulation of fields, circuits, and their interaction, wavelets, time-frequency transforms, and their applications. He is author of more than 120 journal and conference papers. He is co-recipient of the 2007 Best Paper Award of the IEEE Trans. Advanced Packaging. He received the IBM Shared University Research (SUR) Award in 2007, 2008 and 2009. Dr. Grivet-Talocia served as Associate Editor for the IEEE TRANSACTIONS ON ELECTROMAGNETIC COMPATIBILITY from 1999 to 2001.

PLACE PHOTO HERE

Haisheng Hu received B.Sc and M.A.Sc degrees in electronic engineering in 2006 and 2008 respectively, from Harbin Institute of Technology, Harbin, China. He is currently working towards a Ph.D. degree in Electromagnetic Compatibility Group, Politecnico di Torino, Italy. His research interests concern macromodeling of electrical interconnects and related simulation problems. In particular, he works on passive model construction of distributed interconnects and Waveform-Relaxation algorithms.